Neuropeptide-dependent spike time precision and plasticity in circadian output neurons

Bryan Chong[1]†, Vipin Kumar[1]†, Dieu Linh Nguyen[1], Makenzie A. Hopkins[1], Lucia K. Spera[1], Elizabeth M. Paul[1], Anelise N. Hutson[1] and Masashi Tabuchi[1]

Affiliations:

[1]Department of Neurosciences, Case Western Reserve University School of Medicine, Cleveland, OH, United States.

†These authors have contributed equally to this work

Please address correspondence to:

Masashi Tabuchi

Department of Neurosciences, Case Western Reserve University School of Medicine

Robbins Bldg, Room E651, 2210 Circle Dr, Cleveland, OH 44106-4975

Email: masashi.tabuchi@case.edu

Running title: Dh31/Dh44 clock neural coding

Keywords (5 max): Circadian clock, pars intercerebralis; DN1p; Dh31; Dh44.

Word Count: 11,236

Figure Count: 7 Figures and 1 table

Abstract

Circadian rhythms influence various physiological and behavioral processes such as sleep-wake cycles, hormone secretion, and metabolism. Circadian output neurons are a group of neurons that receive input from the central circadian clock located in the suprachiasmatic nucleus of the mammalian brain and transmit timing information to different regions of the brain and body, coordinating the circadian rhythms of various physiological processes. In *Drosophila*, an important set of circadian output neurons are called pars intercerebralis (PI) neurons, which receive input from specific clock neurons called DN1. These neurons can further be subdivided into functionally and anatomically distinctive anterior (DN1a) and posterior (DN1p) clusters. The neuropeptide diuretic hormones 31 (Dh31) and 44 (Dh44) are the insect neuropeptides known to activate PI neurons to control activity rhythms. However, the neurophysiological basis of how Dh31 and Dh44 affect circadian clock neural coding mechanisms underlying sleep in *Drosophila* is not well understood. Here, we identify Dh31/Dh44-dependent spike time precision and plasticity in PI neurons. We find that the application of synthesized Dh31 and Dh44 affects membrane potential dynamics of PI neurons in the precise timing of the neuronal firing through their synergistic interaction, possibly mediated by calcium-activated potassium channel conductance. Further, we characterize that Dh31/Dh44 enhances postsynaptic potentials in PI neurons. Together, these results suggest multiplexed neuropeptide-dependent spike time precision and plasticity as circadian clock neural coding mechanisms underlying sleep in *Drosophila*.

Abbreviations

AHP	afterhyperpolarization
AUC	Area under the curve
CGRP	Calcitonin gene-related peptide
CRF	Corticotropin-releasing factor
CV	coefficient of variation
Dh31	Diuretic hormone 31
Dh44	Diuretic hormone 44
Dilp2	Drosophila insulin-like peptide 2
DN1	Dorsal neuron 1
GMM	Gaussian mixture model
LV	local variation
PCR	Polymerase chain reaction
PDF	pigment-dispersing factor
PFA	paraformaldehyde
PI	Pars Intercerebralis
ROC	receiver operating characteristic
SLOB	slowpoke-binding protein
tdGFP	tandem dimer green fluorescent protein
ZT	zeitgeber time

1 INTRODUCTION

Circadian rhythms are biological processes that follow an approximately 24-hour cycle and are

regulated by an internal biological clock (Brown & Schibler, 1999; Dunlap, 1999; Helfrich-Forster, 2003; Gachon *et al.*, 2004; Green *et al.*, 2008; Nitabach & Taghert, 2008; Buhr & Takahashi, 2013; Hardin & Panda, 2013; Dubowy & Sehgal, 2017; Cedernaes *et al.*, 2019). These rhythms influence various physiological and behavioral processes such as sleep-wake cycles, hormone secretion, and metabolism (Green *et al.*, 2008; Franken & Dijk, 2009; Dallmann *et al.*, 2012; Cedernaes *et al.*, 2019; Hill *et al.*, 2020). Circadian output neurons are a group of neurons that receive input from the central circadian clock located in the suprachiasmatic nucleus of the mammalian brain and transmit timing information to different regions of the brain and body (Sun *et al.*, 2001; Herzog & Schwartz, 2002; Welsh *et al.*, 2010; Colwell, 2011; Mohawk & Takahashi, 2011), coordinating the circadian rhythms of various physiological processes (Hastings *et al.*, 2018; Goltsev *et al.*, 2022). Disruption of clock genes has been linked to sleep disorders and the development of metabolic diseases (Maury *et al.*, 2014; Cedernaes *et al.*, 2019; Cederroth *et al.*, 2019). Conversely, aberrant nutrient signaling can affect circadian rhythms of behavior, suggesting a bidirectional interaction between circadian rhythms and metabolic processes (Huang *et al.*, 2011). The circadian rhythm also interacts with metabolic processes to regulate energy balance, influencing factors such as hormone release, nutrient distribution, and basal metabolic rate (Panda, 2016). DN1 neurons are known to exhibit anatomical and functional heterogeneity, including anterior (DN1a) and posterior (DN1p) clusters. Several non-clock circuits have been identified downstream of DN1p clock neurons, including tuberculo-bulbar neurons(Guo *et al.*, 2018; Lamaze *et al.*, 2018) and a potentially specific class of dopaminergic neurons (Liang *et al.*, 2019). Besides them, there is an important set of circadian output neurons called pars intercerebralis (PI) neurons (Cavanaugh *et al.*, 2014), which receive monosynaptic inputs specifically from DN1 clock neurons (Barber *et al.*, 2016), controlling the circadian regulation of sleep (Guo *et al.*, 2016; Guo *et al.*, 2018; Lamaze *et al.*, 2018; King & Sehgal, 2020; Shafer & Keene, 2021; Tabuchi *et al.*, 2021). The dynamics of the *Drosophila* circadian network involve many types of neuropeptidergic signaling (Schlichting *et al.*, 2016; King *et al.*, 2017; Klose *et al.*, 2021), such as PDF, pigment-dispersing factor (Mertens *et al.*, 2005), leucokinin (Cavey *et al.*, 2016), short neuropeptide F (Shang *et al.*, 2013), ion transport peptide (Hermann-Luibl *et al.*, 2014), and Allatostatin A (Chen *et al.*, 2016), in addition to fast amino acid neurotransmitters such as glutamate (Hamasaka *et al.*, 2007; McCarthy *et al.*, 2011; Tabuchi *et al.*, 2018), GABA (Parisky *et al.*, 2008; McCarthy *et al.*, 2011; Lelito & Shafer, 2012; Gmeiner *et al.*, 2013; Liu *et al.*, 2014), and acetylcholine (Wegener *et al.*, 2004; McCarthy *et al.*, 2011; Lelito & Shafer, 2012). In the context of neuropeptidergic regulation, the neuropeptide diuretic hormones 31 (Dh31) and 44 (Dh44) are homologous to the mammalian calcitonin gene-related peptide (CGRP) and corticotropin-releasing factor (CRF), respectively (Lee *et al.*, 2023a). Similar to the mammalian CGRP, *Drosophila* Dh31 plays key roles in intestinal peristalsis (Benguettat *et al.*, 2018), reproduction (Kurogi *et al.*, 2023), memory formation (Lyu *et al.*, 2023), sleep regulation (Kunst *et al.*, 2014), circadian rhythms (Goda *et al.*, 2019), and temperature compensation (Goda *et al.*, 2016). The conserved functions of Dh31 across species underscore its importance in the regulation of diverse physiological processes. Similarly, Dh44 and CRF are involved in the regulation of stress responses, but also circadian regulation of sleep. Mammalian CRF neurons in the paraventricular nucleus of the hypothalamus are involved in the regulation of sleep and wakefulness, as they are part of the neural circuits that control wakefulness and are influenced by the circadian pacemaker (Ono *et al.*, 2020). In *Drosophila*, Dh44-positive PI neurons have been implicated in the control of rest-activity rhythms (Cavanaugh

et al., 2014; King *et al.*, 2017). Hugin-expressing neurons, which act downstream of clock neurons to regulate rhythmic locomotor activity , are also suggested as a specific neural circuit through which Dh44 influences these behaviors (King *et al.*, 2017; Barber *et al.*, 2021; Schwarz *et al.*, 2021). In addition, like Dh31, Dh44 is involved in several other aspects of physiology, including growth and metabolism (Dus *et al.*, 2015). Dh44 is known to activate PI neurons to control the rhythm of activity, and the reduction of sleep can be activated by nutrient starvation (Oh & Suh, 2023). In the context of the involvement of Dh31 and Dh44 in DN1 and PI neurons, the connections between DN1a and Dh44 neurons are identified in the early third-instars stage (Poe *et al.*, 2023), and multiple pieces of evidence support that DN1p potentially secretes Dh31(Kunst *et al.*, 2014), which might play an important role in modulating PI neurons. However, the neurophysiological and computational basis of how Dh31 and Dh44 affect PI neuron firing, and the resulting neural coding is not well understood. In the present study, we identify synergistic effects of Dh31 and Dh44 in terms of how they influence membrane potential dynamics of PI neurons. We find that such a synergistic interaction between Dh31 and Dh44 contributes to enhancing the reliability of action potential timing and synaptic potentiation that promotes arousal. Taken together, these results suggest a multiplexed neuropeptide-dependent precision and plasticity of spike timing in circadian output neurons as a neural coding mechanism for the circadian clock that underlies sleep in *Drosophila*.

2 MATERIALS AND METHODS

2.1 Fly Strains

The *Drosophila* strains utilized in this study were acquired from the Bloomington Drosophila Stock Center (Bloomington, IN, USA), except for *UAS-slob RNAi* obtained from Vienna Drosophila Research Center (VDRC: 100987). To target and visualize the PI neurons, *Dilp2-Gal4* line (a gift from Amita Sehgal) and *UAS-CD4-tdGFP* line (BDSC: 35836) were recombined through standard genetic recombination techniques to enable use for electrophysiological recordings. We established a split-GAL4 driver by recombining *R20A02-AD* (BDSC: 70582) and *R18H11-DBD* (BDSC: 69017), and *UAS-NaChBac* (BDSC: 9466) and *UAS-dTRPA1* (BDSC: 26263) were used to activate $Dh31^{+}$-DN1p cells targeted by *R20A02-AD;R18H11-DBD*. All strains, with the exception *of R20A02-AD;R18H11-DBD*, were outcrossed into the *iso31* (BDSC: 5905) genetic background at least 4 times. The flies were nourished with standard *Drosophila* food comprising molasses, cornmeal, and yeast. Flies were stocked in a 25°C incubator (DR-36VL, Percival Scientific, Perry, IA, United States) following a 12h:12h light:dark cycle and kept at 65% humidity. All experiments involved female flies (5-8 days old) and were conducted at 25 °C, adhering to all pertinent ethical regulations for animal testing and research at Case Western Reserve University.

2.2 Cell-Free Protein Synthesis

Dh31 and Dh44 DNA were amplified from their template DNA based on gBlocks Gene Fragments (Integrated DNA Technologies) by using UltraRun LongRange polymerase (206442; QIAGEN). For PCR-based amplification of Dh31, 5’-AAAGCGATCGCATGACAAACCGAT-3’ and 5’-GTTTAAACTTAGACATCGGTCTCGG-3’ were used as primers, and for amplification of Dh44, 5’-AAAGCGATCGCATGATGAAAGCCACA-3’ and 5’-GGGCGGTT

TAAACTTAATTAACGTTAT-3' were used as primers. These corresponded to nucleotides 1 to 351 or 3,781 to 4,132 in the Dh31 sequence and corresponded to nucleotides 1 to 1071 or 5,311 to 6,382 in the Dh44 sequence. Amplification was performed by using the following thermal program: 93°C for 3 min; 35 cycles of 95°C for 30 s, 54°C for 30 s, and 65°C for 10 min; followed by one cycle at 72°C for 10 min. The PCR products were separated by electrophoresis on a 1.5% agarose gel. The DNA was extracted from the agarose gel using the GeneJET Gel Extraction Kit (K0691; Thermo Scientific). The samples were purified to reach sufficient concentrations before proceeding to each step. Purification was performed by ethanol precipitation and Wizard SV Gel and PCR Clean-Up System (A9281; Promega). DNA fragments encoding Dh31 and Dh44 were subcloned into the SgfI and PmeI sites of pF25A ICE T7 Flexi Vector (L1061, Promega) available in the kit of the TnT T7 Insect Cell Extract Protein Expression System (L1101, Promega), according to manufacturer instructions. The identities of the subcloned PCR products were verified by Sanger Sequencing analysis by using primers 5'-CGGATGGCCTTTTTGCG TTTCTA-3' and 5'-CTTCCTTTCGGGCTTTGT TAG-3' for Dh31, and 5'-AAAGCGATCGCA TGATGAAAGCCACA-3' and 5'-GGGCGGT TTAAACT TAATTAACGTTAT-3' for Dh44. For protein synthesis, the TnT T7 Insect Cell Extract Protein Expression System was used to allow both transcription and translation to occur in a single reaction. TnT T7 ICE Master Mix was mixed with 4µg of plasmid DNA template and brought up to a volume of 50 µl with nuclease-free water. The reactions were incubated at 30°C for 4 hours to allow protein synthesis to occur. Synthesized Dh31 and Dh44 were stored at -80 °C until use. These synthesized Dh31 and Dh44 were used at a final concentration of 10^{-6} M when they were tested alone (i.e., Dh31 or Dh44), and at a final concentration of 5 x 10^{-7} M when they were tested as a cocktail (i.e., Dh31 and Dh44). Selected concentration was based on previous study (Shafer *et al.*, 2008). As a control vehicle, TnT T7 ICE Master Mix with Luciferase ICE T7 Control DNA was used.

2.3. Membrane-coated glass electrodes

We performed perforated patch-clamp and sharp-electrode electrophysiological recordings from a PI neuron using membrane-coated glass electrodes (Jameson *et al.*, 2024). We used a perforated patch clamp in order to acquire action potential firing with current-clamp mode and KCa currents with voltage-clamp mode. On the other hand, we used sharp-electrode electrophysiological recordings to acquire synaptic potentials to obtain signals within the axonal regions under tonic hyperpolarization current injection, which is hard to hold with the patch clamp technique. We used membrane-coated glass electrodes to make recording more stable as we found that membrane-coated glass electrodes were helpful for suppressing artifactual signal variability, which is derived from mainly access resistance fluctuations during the recording (Jameson *et al.*, 2024). A lipid membrane was created with the use of 7.6 g/L egg yolk lecithin (440154; Sigma-Aldrich) and 2 mM cholesterol (C8667; Sigma-Aldrich) by dissolving with hexane solvent (34859; Sigma-Aldrich) and acetone (270725; Sigma-Aldrich) for one hour at room temperature using an ultrasonication machine, as previously described (Jameson *et al.*, 2024). Hexane and acetone were evaporated through pressure injection of inert nitrogen, followed by an additional incubation under the decompression chamber. The hexane/acetone solvent was entirely removed, and the egg yolk lecithin and cholesterol were transferred to a mixture of liquid paraffin/squalene (7/3, v/v), then incubated at 80°C overnight. The following day, the prepared lipid was promptly utilized for electrode preparation. Patch-electrodes (12 − 20 MΩ) were formed using a Flaming-Brown puller

(p-97; Sutter Instrument, CA, USA with thoroughly cleaned borosilicate glass capillaries (OD/ID: 1.2/0.68mm). The electrode tip was refined with a microforge (MF200; World Precision Instruments, FL, USA). Sharp-electrodes (120 − 190 MΩ) were formed using a laser-based micropipette puller (P-2000, Sutter instrument) with thoroughly cleaned quartz glass capillaries (OD/ID: 1.2/0.6mm). These electrodes were coated with the prepared phospholipids using a tip-dip protocol (Jameson *et al.*, 2024). Briefly, we initially dipped the electrode tip into an internal electrode solution in a custom-made reservoir, and then the prepared lipid solution was loaded onto the surface of the internal electrode solution. Following the application of the minimum amount (<20 μL) of prepared lipid solution onto the surface of the internal electrode solution, the electrode was vertically lifted using a micromanipulator. The electrode was prepared for electrophysiological recording through standard backfilling of the internal electrode solution by using a microfiller (MF34G MicroFil; World Precision Instruments). The internal pipette solution loaded into the tip contained 102 mM potassium gluconate, 0.085 mM $CaCl_2$, 0.94 mM EGTA, 8.5 mM HEPES, 4 mM Mg-ATP, 0.5 mM Na-GTP, 17 mM NaCl, pH7.2 and was utilized for all patch-clamp recording experiments. For sharp electrode intracellular recordings, a 1 M KCl internal pipette solution was loaded into the pipette. Filtering of the internal pipette solutions were performed using a syringe filter with a pore size of 0.02 μm (Anotop 10, Whatman).

2.4. Preparation

In vivo preparation for electrophysiology of PI neurons was performed as previously described (Tabuchi *et al.*, 2018). To anesthetize the flies, they were chilled for 10 min and glued to a 0.025 mm thick metal shim using dental wax or UV light cure adhesives. The cuticle was then peeled off to expose the surface of the brain, and the tethered fly was mounted in a chamber containing *Drosophila* physiological saline (101 mM NaCl, 3 mM KCl, 1 mM $CaCl_2$, 4 mM $MgCl_2$, 1.25mM NaH_2PO_4, 20.7 mM $NaHCO_3$, and 5 mM glucose; with osmolarity adjusted to 235-245 mOsm and pH 7.2), which was pre-bubbled with 95% O_2 and 5% CO_2. The large trachea and intracranial muscles were removed. The glial sheath surrounding the PI neurons was carefully removed using sharp forceps following the treatment of the enzymatic cocktail, collagenase (0.1 mg/mL), protease XIV (0.2 mg/mL), and dispase (0.3 mg/mL), at 22°C for one minute, which is essentially the same condition when we conduct electrophysiological recordings from DN1 neurons. A small stream of saline was repeatedly pressure-ejected from a large-diameter pipette to clean the surface of the cell body under a dissection microscope. The PI neurons were visualized via tdGFP fluorescence by utilizing the PE4000 CoolLED illumination system (CoolLED Ltd., Andover, UK) on a fixed-stage upright microscope (BX51WI; Olympus, Japan).

2.5. Patch-clamp electrophysiology

Perforated patch-clamp was conducted using somatic recording, following procedures described in previous studies (Nguyen *et al.*, 2022; Jameson *et al.*, 2024). Escin was prepared as a 50 mM stock solution in water and was added fresh to the internal pipette solution, achieving a final concentration of 50 μM. To prevent light-induced changes, the filling syringes were wrapped with aluminum foil due to the light-sensitivity of escin. The escin pipette solutions demonstrated stability for several hours after mixing in the filling syringe, with no observable formation of precipitates. Junction potentials were nullified before the formation of a high-resistance seal formation. Perforated patches were allowed to spontaneously develop over time following the

high-resistance seal formation. Once breakthrough was apparent, indicated by the gradual development of a large capacitance transient in the seal test window, monitoring of access resistance was initiated using the membrane test function. From that point onward, access resistance (Ra) was continuously monitored throughout the final stages of the perforation process until it stabilized (Ra stably < 40 MΩ). To isolate KCa currents, we perfused saline containing 10^{-7} M Tetrodotoxin to block voltage-gated sodium currents and 4×10^{-3} M 4-Aminopyridine to block fast-inactivated voltage-gated potassium currents (Tabuchi *et al.*, 2018). The PI neurons were held at −70 mV and two series of 200-ms voltage pulses were delivered in 10-mV increments between −80 and 60 mV. The second series was recorded with saline containing 5×10^{-4} M $CdCl_2$, which abolished voltage-activated Ca^{2+} currents. The subtraction of the current trace in the presence of 5×10^{-4} M $CdCl_2$ from the current trace without 5×10^{-4} M $CdCl_2$ was defined as KCa current. Axopatch 1D amplifier (Molecular Devices) was utilized in obtaining electrophysiological signals, which were then sampled with Digidata 1550B (Molecular Devices) under the control of pCLAMP 11 (Molecular Devices). The electrophysiological signals were sampled at 20 kHz and subjected to a low-pass filter at 1 kHz. To characterize Dh31 and Dh44 inducible responses, we perfused apamin (10^{-5} M) and/or cadmium (10^{-4} M) together with Dh31 and Dh44 (Jedema & Grace, 2004).

2.6. Sharp electrode intracellular recordings

Intracellular recording was performed by inserting sharp microelectrodes as described in previous studies (Nguyen *et al.*, 2022; Jameson *et al.*, 2024). We utilized this method in order to acquire stable synaptic potential under tonic hyperpolarization current injection. The electrode was introduced into the region characterized by dense tdGFP signals within the axonal regions of PIs in *Dilp2-Gal4>UAS-CD4-tdGFP* flies. During the insertion of the electrode, tdGFP signals served as the basis for initial visual inspection, while the depth of insertion was directed by alterations in sound (Model 3300 Audio Monitor, A-M Systems) and the generation of membrane potential. To facilitate this process, "buzz" pulses were added just before the electrode was ready to cross the membrane. The duration of the pulse was determined by a technique called "advance air shooting". If the microscope revealed that the electrode tip was physically shaking, the duration was considered excessive. We utilized the longest duration in the range where the electrodes remained stationary, typically between 2-5 ms. Commencement of membrane potential recordings occurred once the membrane potential had stabilized, typically requiring several minutes. Recordings were conducted with an Axoclamp 2B with HS-2A x 1 LU headstage (Molecular Devices), and sampled with Digidata 1550B interface, controlled by pCLAMP 11 software on a computer. The signals were sampled at 10 kHz and subjected to a low-pass filter at 1 kHz.

2.7. Immunostaining

Brains or thoracic ganglion were fixed in 4% PFA at 4°C overnight. After several washes with phosphate-buffered saline (137 mM NaCl, 2.7 mM KCl, 10 mM Na_2HPO_4, 1.7 mM KH_2PO_4) + 0.3% Triton X-100 (PBST), samples were incubated with rabbit anti-GFP (Thermo Fisher, 1:200) and mouse anti-BRP (nc82, Developmental Studies Hybridoma Bank, 1:50) at 4°C overnight. After additional PBST washes, samples were incubated with Alexa488 anti-rabbit (Thermo Fisher, 1:1000) for anti-GFP staining and Alexa568 anti-mouse (Thermo Fisher, 1:1000) for anti-BRP

stainings overnight at 4°C. After another series of washes in PBST at room temperature over 1 hr, samples were cleared in 70% glycerol in PBS for 5 min at room temperature and then mounted in Vectashield (Vector Labs). Confocal microscope images were taken under 10x or 63x magnification using a Zeiss LSM800.

2.8. Sleep behavioral assay

Sleep behavior was measured with the use of consolidated locomotor inactivity, as described previously (Tabuchi *et al.*, 2018). Female flies (5-8 days old) were loaded into glass tubes containing 5% sucrose and 2% *Drosophila* agar medium. Fly behavior was monitored using the *Drosophila* activity monitors (DAM, Trikinetics, Waltham, MA) in an incubator at 25°C with a 12 hr:12 hr light:dark (LD) cycle for 2 days to measure sleep. The first day following loading was not included in the analysis. Activity counts were collected in 1 min bins, and sleep was identified as periods of inactivity of at least 5 min. Sleeplab (Joiner *et al.*, 2006), a MATLAB-based (MathWorks) software, was used to quantify sleep behavior.

2.9. Data analysis and statistics

Statistical analyses were done using Prism software version 10.1.0. (GraphPad), Clampfit version 10.7 (Molecular Devices) or MATLAB 2023b (MathWorks). For comparisons of two groups of normally distributed data, unpaired t-tests were used. Paired t-tests were applied for comparisons of electrophysiological signals with normal distributions from the same neuron, before and after stimulation. For comparisons between multiple groups, either one-way ANOVA with post hoc Tukey test or Kruskal-Wallis test with Dunn's multiple comparisons test was used for normally distributed and non-normally distributed data, respectively. A significance threshold of p-value < 0.05 denoted statistically significant test results while asterisks indicated varying levels of significance (*p < 0.05, **p < 0.01, ***p < 0.001, and ****p < 0.0001). Error bars represent means ± SEM averaged across experiments. The reliability of the spike onset was calculated using Cronbach's alpha, as previously described (Tabuchi *et al.*, 2018). Cronbach's alpha is defined as

$$\alpha = \frac{k\bar{c}}{\bar{v}(k-1)\bar{c}}$$

Where k represents the number of action potentials, $\bar{v}$ represents the average variance of action potential onset rapidness slope, which was defined by dVm/dt measured from spike onset threshold to peak dVm/dt, and $\bar{c}$ represents the average inter-dataset covariance of action potential onset rapidness slope.

To quantify spike pattern, the coefficient of variation (CV) and CV2 of interspike intervals (ISI) were used (Holt *et al.*, 1996). CV reflects a global measure of irregularity and is defined as

$$CV = \frac{\sigma_{\Delta t}}{\langle \Delta t \rangle}$$

where σ is the standard deviation of ISI and μ is the average time of ISI.

CV2 indicates a local measure of irregularity defined as the dispersion of the adjacent ISIs. Thus, CV2 is defined as

$$CV2 = \frac{2|\Delta t_{i+1} - \Delta t_i|}{\Delta t_{i+1} + \Delta t_i}$$

where Δt is an interval time of the *ith* ISI.

We also calculated the local variation (LV) as alternative measures of local irregularity, by computing the dispersion of the two adjacent ISIs. LV is defined as

$$Lv = \frac{1}{n-1}\sum_{i=1}^{n-1}\frac{3(ISI_i - ISI_{i+1})^2}{(ISI_i + ISI_{i+1})^2}$$

where ISI_i is the *ith* ISI and n is the number of ISIs (Shinomoto *et al.*, 2003). While both CV2 and LV compare successive ISIs, they provide different perspectives on spike train variability. CV2 is a measure of overall ISI variability, while LV focuses on the local irregularity of ISI sequences. LV is specifically designed to detect variations in local firing patterns that CV2 may miss, especially in non-Poissonian processes (Shinomoto *et al.*, 2009). Although the results for CV2 and LV may appear similar, the inclusion of both metrics is critical for a more complete analysis. CV2 provides insight into general ISI variability, while LV highlights local variations that are important for understanding subtle differences in firing patterns that may not be captured by CV2 alone. Thus, both metrics complement each other to provide a more robust characterization of neural activity.

To visualize local spike variability, we used a Gaussian Mixture Model (GMM) as described previously (Tabuchi *et al.*, 2018). GMM assumes that data points arise from a mixture of Gaussian distributions, each defined by its mean and covariance matrix. Model parameters, including mixture weights and Gaussian component parameters, were estimated using the Expectation-Maximization (EM) algorithm. To preprocess the data, interval timings of PSPs were normalized by the cell-average firing rates and aggregated across cells. Second-order distributions were then constructed by logarithmically binning adjacent pairs of normalized intervals into a 2D histogram. Specifically, we utilized a grid of 22 x 22 bins. For different conditions, distinct logarithmic ranges were employed. We fitted 3 to 5 Gaussian components with full covariance to the joint second-order distributions. For validation purposes, we generated size-matched random samples from the model, producing joint and marginal distributions that closely resembled the training data. To create rate-matched pairs, we first sampled an average PSPs frequency from a beta distribution fitted to the PSPs of PI neurons at ZT18-20. Subsequently, we iteratively constructed novel PSPs trains by selecting the next interval based on the current interval, continuing until the required number of PSPs was reached. Interval selection was performed via rejection sampling of the continuous conditional probability densities of the GMM, following the exclusion of 200 burn-in samples. The resulting logarithmic intervals were exponentiated and normalized to yield PSP times, which were then binned into 10 ms binary signals. To assess the processing performance of the synaptic transmission, we used the area under the curve (AUC) in receiver operating characteristic (ROC) analysis. The AUC in ROC analysis provides a single scalar value that summarizes the performance of a classification model across different thresholds, reflecting the model's ability to discriminate between different classes, making it a useful metric for assessing processing power in tasks where discrimination is important (Hajian-Tilaki, 2013). A model with an AUC close to 1 indicates strong discriminative power, while an AUC close to 0.5 indicates random guessing

(Corbacioglu & Aksel, 2023). Defining performance based on AUC provides a clear and interpretable measure of model effectiveness. We used the 8900 convergence ratios (from $\delta = 0.01$ to $\delta = 0.9$) of presynaptic to postsynaptic transmission as 8900 input arguments to the ROC analysis.

3 RESULTS

3.1 Dh31/Dh44 induced change in action potential firing

The synapses between DN1 circadian clock neurons and PI neurons play a critical role in translating circadian rhythms into physiological outputs. We used this connection as a model to study multiplexed neuropeptide mechanisms because this synapse is where Dh31 and Dh44 signaling cross. To access this synapse, we used an in vivo preparation in which the postsynaptic PI neurons are genetically labeled (Figure 1a). We focused on ZT18-20 as a specific time window for our electrophysiological recordings because this time window is associated with high-quality sleep during the night, which is supported by a steady state of stable neural dynamics of DN1 circadian clock neurons. PI neurons have less spontaneous firing activity during the night, and ZT18-20 has a particularly low rate of spontaneous firing frequency, which is close to 0 Hz (Tabuchi, 2018). Despite the physical disturbances associated with live dissections of the samples, which is required for our recordings, we find the PI neuron's clock function is not disrupted. Since both Dh31 and Dh44 are associated with arousal promotion, we hypothesized that bath application of Dh31 and Dh44 would cause an increase in firing activity of PI neurons. We performed cell-free protein synthesis of Dh31 and Dh44 and applied the synthesized Dh31 and Dh44 to PI neurons (Figure 1b). Compared to the control (Figure 1c), spontaneous firing of PI neurons during ZT18-20 increased with the application of Dh31 alone (Figure 1d), Dh44 alone (Figure 1e), and Dh31 and Dh44 together (Figure 1f). We found that a mixture of Dh31 and Dh44 evoked supralinear firing of PI neurons (Figure 1f). In contrast to the spontaneous firing rate, we did not find significant changes in the resting membrane potential (Figure 1g–j). Next, we quantified intrinsic membrane excitability by current injection (Figure 2a). Similar to spontaneous firing, while Dh31 and Dh44 alone showed almost similar levels of evoked firing frequency (Figure 2b–d), evoked firing activity showed a supralinear increase in that a mixture of Dh31 and Dh44 strongly increased evoked firing frequency. (Figure 2e). Together, these data suggest that Dh31 and Dh44 synergistically interact to enhance action potential firing of PI neurons during ZT18-20.

3.2 Dh31/Dh44 induced action potential waveform change

To investigate the biophysical origins underlying the Dh31/Dh44-induced change in action potential firing, we analyzed the kinetics of the action potential waveform (Figure 3a). We focused on analyzing action potential waveforms from spontaneous firing because the kinetics were artifactually distorted in evoked firing (Figure 2a), which is commonly observed in invertebrate unipolar neurons due to the distance between the current injection site and the action potential generation site (Gouwens & Wilson, 2009). The action potential waveforms exhibit variation induced by interactions with Dh31, Dh44, Dh31/Dh44, Dh31/Dh44 with apamin (10^{-5} M), and Dh31/Dh44 with cadmium (10^{-4} M). Cadmium and apamin were used to selectively inhibit calcium and SK channels, respectively (Jedema & Grace, 2004). While the amplitude and threshold of action potentials were not significantly different in the presence of Dh31/Dh44 (Figure

3b, c), greater afterhyperpolarization (AHP) amplitude was induced by Dh31/Dh44 (Figure 3d). Interestingly, the change in AHP amplitude was only sensitive to cadmium but not apamin. Based on the potential relationship between action potential waveforms kinetics and firing precision (Axmacher & Miles, 2004; Naundorf *et al.*, 2006; Niday & Bean, 2021), we quantified the reliability of action potential timing by using internal consistency of onset rapidness (Tabuchi *et al.*, 2018), which we computed using Cronbach's alpha. Reliability was found to be influenced across all applications with a significant reduction induced by cadmium (Figure 3e).

3.3 Dh31/Dh44 induced spike pattern change and KCa channel conductance

AHP amplitude is closely related to spike patterns in neuronal cells (Scuri *et al.*, 2005; Stiefel *et al.*, 2013; Dumenieu *et al.*, 2015; Trinh *et al.*, 2019; Cui *et al.*, 2022). To investigate whether Dh31/Dh44 applications also influence spike patterns, we analyzed spike frequency adaptation, which is one of the mechanisms shaping spike patterns. The spike frequency adaptation was quantified from the ratio of the 1st ISI to the nth ISI, and an index value closer to 1 would indicate that no spike adaptation occurred, whereas an index value closer to 0 would indicate significant spike adaptation with prolongation of the ISIs (Figure 4a). The Dh31/Dh44 interact and convey significant spike irregularity compared to Dh31 alone and Dh44 alone (Figure 4b–d). CV (Figure 4b), LV (Figure 4c), and CV2 (Figure 4d) each provide complementary information about the temporal structure of neuronal spike trains: CV is sensitive to changes in the overall firing rate, but LV is a measure of variability in the timing of spikes within local time windows, and CV2 is a measure of spike irregularity that considers pairs of consecutive ISIs. Nevertheless, we found that the application of cadmium and apamin decreased Dh31/Dh44-enhanced spiking irregularity in all metrics (Figure 4b–d). One of the contributing factors in shaping AHP and spike patterns can be KCa channel conductance (Engbers *et al.*, 2012; Stiefel *et al.*, 2013; Sahu & Turner, 2021), and KCa channels are known to play a critical role in shaping the activity rhythms of PI neurons (Ruiz *et al.*, 2021). Therefore, we directly quantified KCa channel conductance in PI neurons by voltage-clamp recordings (Figure 4e). We found that K_{Ca} conductance amplitude was increased when Dh31 and Dh44 interacted with each other (Figure 4f, g). SLOB (slowpoke-binding protein) is known as a key mediator in modifying K_{Ca} conductance(Shahidullah *et al.*, 2009; Jepson *et al.*, 2013). Thus, we tested if genetic manipulation of SLOB in PI neurons changes Dh31/Dh44-induced changes in K_{Ca} conductance. Strikingly, we found that Dh31/Dh44-induced changes in K_{Ca} conductance was completely eliminated by introducing SLOB RNAi in PI neurons (Figure 4h, i). These results suggest that Dh31/Dh44-induced changes in K_{Ca} conductance were mediated by SLOB in PI neurons.

3.4 Dh31/Dh44 induced changes in synaptic properties

To reveal if Dh31/Dh44 impacted synaptic drive, we examined postsynaptic potential (PSP) parameters such as amplitude, inter-event interval, cumulative probability, and probability density. The voltage traces of PSPs are altered when Dh31 and Dh44 were introduced, with high increased activity when both Dh31/Dh44 were present (Figure 5a). The cumulative probability varied for each condition when recording across PSP amplitudes (Figure 5b). The amplitude of PSP for the condition with both Dh31 and Dh44 was significantly greater compared to the control (Figure 5c).

Amplitude changes in PSP generally reflect postsynaptic changes in response to neurotransmitters (Turrigiano *et al.*, 1998), and we next asked whether the frequency of PSP, which is more related to presynaptic events, was changed. We found that PSP inter-event interval was quantified and the Dh31/Dh44/apamin was significantly different from all other conditions (Figure 6b). The probability density during PSP inter-event intervals for the Dh31/Dh44 and Dh31/Dh44/apamin groups was decreased (Figure 6a). Taken together, these data suggest that Dh31 and Dh44 interact synergistically to enhance the PSPs of PI neurons, which may be mediated by both presynaptic and postsynaptic manners.

3.5 Dh31/Dh44 enhances temporal patterns of synaptic potentials and possible involvement of Dh31-positive DN1 clock neurons

To identify the computational basis for how Dh31/Dh44 alters the temporal dynamics of synaptic potentials, we implemented two types of computational models. We first used a Gaussian Mixture Model (GMM). Interval timings of two adjacent PSPs were projected into two-dimensional space, and GMM was used to estimate the geometry of their probability distribution (Figure 6c). We found the emergence of an additional cluster in the presence of Dh31 or Dh44 compared to the singular cluster in the control. Furthermore, in the presence of Dh31 and Dh44, we found the emergence of multiple clusters which was partially diminished by the administration of apamin. We next conducted receiver operating characteristic (ROC) to estimate the processing performance of interval timing of postsynaptic activity of PI neurons. The higher the area under the curve (AUC) in the ROC analysis, the higher the discriminative power, while an AUC close to 0.5 indicates a random chance level (Corbacioglu & Aksel, 2023). We found that the interval timing of PSPs in the presence of Dh31 or Dh44 alone showed higher AUC compared with the control, but their AUC was lower than the interval timing of PSPs in the presence of both Dh31 and Dh44 with the effect partially reduced by apamin (Figure 6d). DN1 clock neurons are known to be one of the major presynaptic inputs to PI neurons (Barber *et al.*, 2016; Tabuchi *et al.*, 2018), and the subset of DN1 clock neurons expressing Dh31 is known to promote wakefulness (Kunst *et al.*, 2014). DN1 clock neurons are known to be heterogenous in their role of promoting sleep and/or wakefulness (Guo *et al.*, 2018; Lamaze *et al.*, 2018), so we decided to establish a split-GAL4 driver to define Dh31-DN1ps neurons. *R20A02-AD* expresses the p65 activation domain associated with Dh31, and *R18H11-DBD* expresses the DNA binding domain of GAL4 associated with PDF receptors (Dionne *et al.*, 2018). Thus, we used *R20A02-AD;R18H11-DBD* as an intersectional approach to genetically extract a putative subset of $Dh31^{+}$-DN1p clock neurons. We found that *R20A02-AD;R18H11-DBD>UAS-thGFP* flies label DN1p cells (5.1 cells ± 1.5, N=90 brains) and a few uncharacterized cells in VNC (Figure 6e). To investigate the potential involvement of Dh31-positive DN1 clock neurons, we first assessed whether genetic neural activation in *R20A02-AD;R18H11-DBD* flies would lead to changes in sleep and activity patterns using *UAS-NaChBac*. (Figure 7a). No significant difference in daytime (ZT0-12) sleep was found, but a significant decrease in nighttime (ZT12-24) sleep was found in flies expressing *UAS-NaChBac* in putative Dh31-DN1ps (Figure 7b). We also found an increase in sleep bout number during nighttime in flies expressing *UAS-NaChBac* in putative Dh31-DN1ps (Figure 7c). We also analyzed locomotor profiles (Figure 7d) and found increases in both nighttime activity time (Figure 7e) and activity level (Figure 7f) were observed in flies expressing *UAS-NaChBac* in putative Dh31-DN1ps; it is possible that the expression of NaChBac drove hyperactivity. Constitutive expression of *UAS-*

NaChBac can cause artifactual effects not only during experiments but also during development. To exclude this possibility, we also performed acute activation of Dh31-DN1ps based on Thermogenics. As a thermogenic tool, we used dTRPA1, a temperature-sensitive ion channel, which can be activated by raising the temperature (Hamada *et al.*, 2008). We found that activation of putative Dh31-DN1ps neurons by temperature elevation significantly reduced sleep of *R20A02-AD;R18H11-DBD>UAS- dTRPA1* flies (Figure 7g), both during the day and at night (Figure 7e), and facilitated sleep fragmentation as evidenced by an increase in the number of sleep bouts (Figure 7i). We also analyzed activity profiles (Figure 7j) and found an increase in active time during nighttime (Figure 7k), but we found daily activity level during wakefulness was reduced, which was opposed to chronic activation of putative Dh31-DN1ps by expressing NaChBac (Figure 7l). We also quantified activity and sleep profiles of flies having *UAS- dTRPA1* alone, without *R20A02-AD;R18H11-DBD* , but we did not find any significant difference compared to control (Figure S1).

4 DISCUSSION

The synapses between circadian clock neurons and circadian output cells play a crucial function in translating circadian rhythms into physiological outcomes, regulating internal drives like sleep and hunger. While many molecules that act as output pathways of the circadian clock have been identified, the mechanistic process of how these molecules alter the actual physiology of the network that generates rhythmic internal drives has remained elusive. We show that two types of neuropeptides synergistically interact to modulate circadian clock neural coding. The induced change in action potential firing in PI neurons from ZT18-20 should indicate an intrinsic membrane excitation change caused by Dh31 and Dh44. We found the effects only on firing rate, but not on resting membrane potential (Figures 1 and 2). This may indicate that their synergistic mechanisms do not directly come from voltage-dependent conductance, which made us infer that implementing a supplementary pharmacological approach would prove advantageous. Thus, we show that biophysical parameters of the action potential waveform estimate which channels are involved by using apamin and cadmium. The results showed a significant difference in amplitude and threshold in the Dh31/Dh44/apamin and Dh31/Dh44/cadmium groups (Figure 3). Cadmium caused a significant decrease in AHP amplitude. Previous research has shown that apamin specifically blocks SK channels, while cadmium has a broader inhibitory effect (Jedema & Grace, 2004), blocking numerous KCa channels, including SK channels (Tabuchi et al., 2018**)**. From our data (Figure 3), we find that only cadmium is having a significant inhibitory effect on neuropeptides, indicating that KCa channels other than SK channels are likely to be the primary effectors. This change suggests that calcium-activated signaling is effective in accelerating repolarization, making the group of neurons susceptible to repetitive firing. We propose that a greater AHP amplitude more effectively resets the membrane potential, leading to quicker recovery and potentially enabling a higher frequency of action potentials. In fact, similar findings have been reported in the mammalian SCN (Cloues & Sather, 2003). We found that greater AHP amplitude induced a change in the availability of voltage-gated conductance for action potential generation, which may be related to a possible mechanism to explain the observed change in amplitude and threshold, suggesting that all the observed changes in action potential waveform kinetics may be related. Because SLOB is known to modulate KCa in both DN1 (Tabuchi *et al.*, 2018) and PI neurons (Shahidullah *et al.*, 2009; Jepson *et al.*, 2013), it is possible that SLOB might

be associated with Dh31/Dh44 signaling, and we assess this possibility by directly measuring KCa currents, which have functions that are related to circadian outputs (Ruiz *et al.*, 2021) and critical period (Lowe *et al.*, 2024).

We next demonstrate that the reliability of the action potential of PI neurons is enhanced by the presence of Dh31 and Dh44 (Figure 3e), and spike irregularity is also enhanced by the presence of Dh31 and Dh44 (Figure 4). The simultaneous induction of increased "reliability" and "irregularity" may seem to be a contradiction. Although neuronal firing is often characterized by irregularity, this doesn't necessarily mean that it is random (Kostal & Lansky, 2007; Kostal *et al.*, 2007; Brette, 2015). Instead, this variability in firing rates can encode important information and reflect the complex dynamics of neural circuits (Kostal & Marsalek, 2010; Waschke *et al.*, 2017; Tomar & Kostal, 2021). Our other observation of spike frequency adaptation of PI spiking induced by Dh31 and Dh44 (Figure 3a) further supports this assertion, as spike frequency adaptation is known to enhance the processing performance of information (Benda *et al.*, 2005; Salaj *et al.*, 2021; Lee *et al.*, 2023b) by making the brain not only processes information effectively, but does so in a way that maximizes the impact of its output on perception and behavior. If irregularity does not necessarily imply randomness, but rather "structured irregularity", then it is possible that increased reliability is essential for the formation of such structured irregularity (Shinomoto *et al.*, 2009; Yang *et al.*, 2017; Tabuchi *et al.*, 2021; Tabuchi, 2024), which is the idea that the irregularity of neural activity patterns is precisely structured rather than being based on randomness (Chini *et al.*, 2022).

In addition to altering action potentials, Dh31 and Dh44 also altered postsynaptic potentials (PSPs) in the PI neurons. We find that both the amplitude and frequency of the PSP epoch were altered by Dh31 and Dh44, suggesting their impacts on both presynaptic and postsynaptic effects. Although retrograde synaptic signaling in the *Drosophila* central synapse has not been thoroughly investigated, it is possible that there is retrograde synaptic signaling related to Dh31 and Dh44 in DN1-PI synapses, as in mammalian synapses (Maejima *et al.*, 2001; Wilson & Nicoll, 2001). We also find that PSPs are not only significantly enhanced in both amplitude and frequency, but also show more complex temporal structures (Figure 6c). Through the GMM-based visualization of these temporal neural activity patterns (Figure 6c), we are able to highlight the multidimensional nature in geometry of neural computation. Theoretical predictions support that such an enhancement is computationally powerful for the precise encoding of information (Levakova *et al.*, 2016), and our ROC computational models support this as well (Figure 6d). Even if such theoretical predictions were true, would it be worthwhile to improve the accuracy of neural operations in such a way on millisecond time scales, especially in systems that do not perform fast information processing (such as sensory input), such as circadian clock neurons? Circadian clock neurons must accurately track and represent time at various scales, ranging from milliseconds to hours. Precise encoding across shorter time intervals allows the neurons to cumulatively aggregate these intervals into longer periods, including hours. This accumulation of precise coding spanning several time scales ultimately may contribute to the regulation of sleep/wake cycles by fractal patterns that persist across these hierarchical scales (Hausdorff & Peng, 1996). This hierarchical organization in time perception and regulation may also extend to the internal computations performed by the brain, wherein neuropeptides play a pivotal role in shaping these dynamic processes (Wu *et al.*; Mountoufaris *et al.*, 2024).Our results in the present study also support this

idea and explain the computational basis of internal state representations based on neural dynamics shaped by multiple neuropeptides. These features of circadian neural coding induced by Dh31 and Dh44 may be behaviorally advantageous for triggering rapid sleep-wake state transitions, particularly when switching from a stable sleep state during the night to a wake state by promoting arousal.

There are several potential limitations to this study. First, we still do not know if Dh31-DN1ps play an important role in Dh31/Dh44 clock neural coding. It is possible that Dh31, deriving from other neurons, plays dominant functions (Goda *et al.*, 2019). The same applies to Dh44 in this context. Because PI neurons used in this study are based on *Dilp2-Gal4* line, other types of PI neurons might be responsible for releasing Dh44 (Ruiz *et al.*, 2021). If this is the case, Dh44 mechanisms might be based on paracrine signaling rather than autoregulation. Second, it is possible that Dh31/Dh44 signaling is not directly related to the synapse between DN1 and PI neurons, but rather indirectly affected via networks such as Hugin^{+} neurons and/or LNd cells (King *et al.*, 2017; Barber *et al.*, 2021; Schwarz *et al.*, 2021). Addressing these issues may provide more valuable insight into mechanistic frameworks on how Dh31/Dh44 signaling is influencing circadian clock neural coding mechanisms. Taken together, our results demonstrate multiplexed neuropeptide-dependent spike time precision and plasticity as a potential neural coding mechanism of the circadian clock underlying sleep in *Drosophila.*

DATA AVAILABILITY STATEMENT

The data that support the findings of this study are available from the corresponding author upon reasonable request.

AUTHOR CONTRIBUTIONS

MT designed the study. BC, VK, DLN, LKS, EMP, ANH, and MT performed the experiments. BC, VK, DLN, MAH, LKS, EMP, ANH, and MT conducted data analysis. BC and MT wrote the manuscript with input from VK, DLN, MAH, LKS, EMP, and ANH.

FUNDING

This work was supported by grants from the National Institutes of Health (R00NS101065 and R35GM142490), Whitehall Foundation, BrightFocus Foundation (A2021043S), PRESTO grant from Japan Science and Technology Agency (JPMJPR2386), and the Tomizawa Jun-ichi and Keiko Fund of the Molecular Biology Society of Japan for Young Scientists.

CONFLICT OF INTEREST STATEMENT

The authors declare that the research was conducted in the absence of any commercial or financial relationships that could be construed as a potential conflict of interest.

ACKNOWLEDGEMENTS

We thank Keisuke Sakurai for the loan of electrophysiological equipment, and Joseph Monaco for technical advice on computational modeling. We also thank Ben Strowbridge, Heather Broihier, and Dominique Durand, along with members of the Tabuchi lab for discussion, and the Light Microscopy Imaging Core at Case Western Reserve University for help with confocal microscopy.

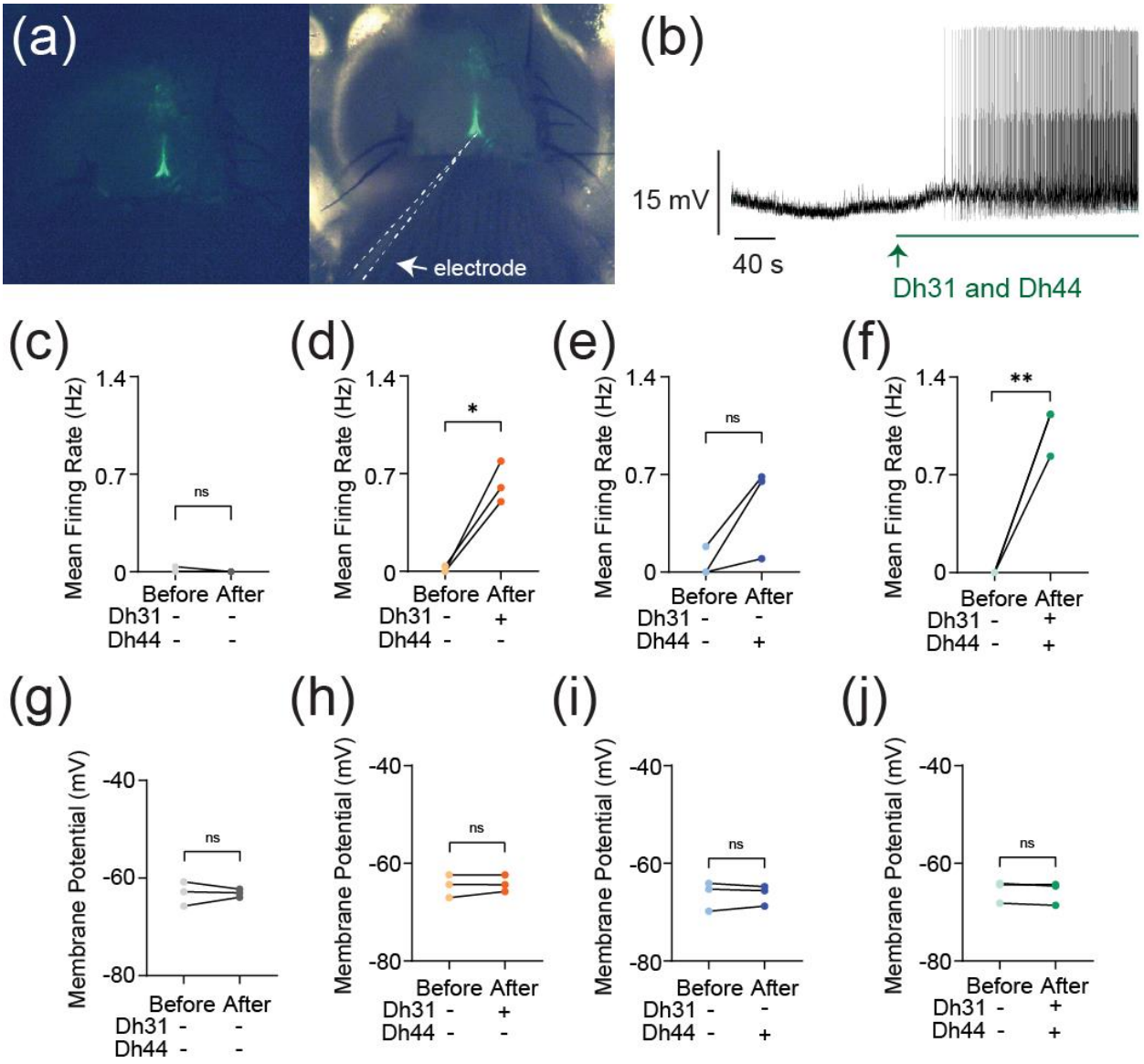

FIGURE 1

FIGURE 1 Change in action potential firing induced by Dh31/Dh44. **(a)** Representation of in vivo expression of the PI neurons through genetic labeling in the brain of the *Drosophila*. **(b)** Voltage trace during the application of synthesized Dh31 and Dh44 to the PI neurons during patch-clamp

recording. **(c-f)** Spontaneous firing of PI neurons during ZT18-20 by using control, with (+) Dh31 (N=3) and without (-) Dh31 (N=3), with (+) Dh44 (N=3) and without (-) Dh44 (N=3) and a combination of Dh31 and Dh44 (N=3). **(g-j)** Resting membrane potential of the PI neurons using control, with (+) Dh31 (N=3) and without (-) Dh31 (N=3), with (+) Dh44 (N=3) and without (-) Dh44 (N=3) and a combination of Dh31 and Dh44. The statistics used were paired t-test with *p < 0.05 and **p < 0.01 and ns indicated non-significant.

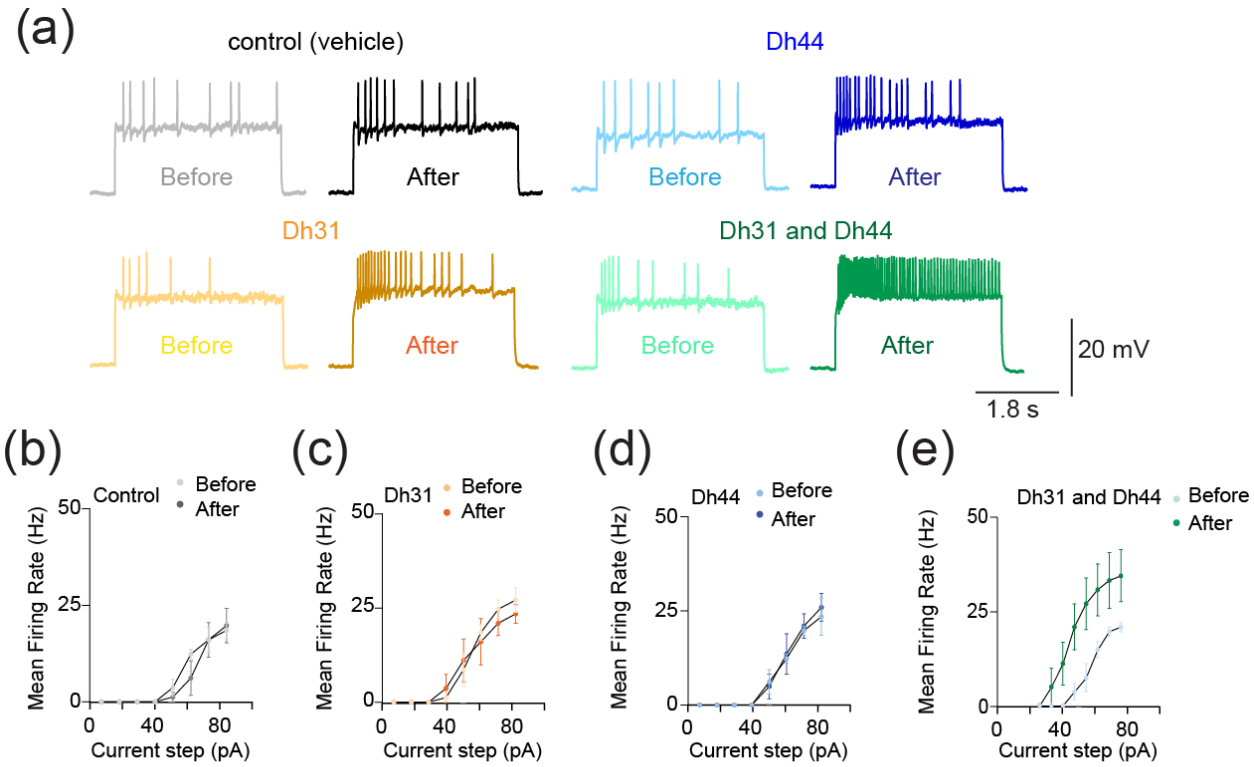

FIGURE 2

FIGURE 2 Change in evoked action potential firing induced by Dh31/Dh44. **(a)** Voltage trace before and after the application of synthesized Dh31 and Dh44 to the PI neurons during patch-clamp recording. **(b-e)** Evoked firing frequency by current injection with control, Dh31, Dh44, and a combination of Dh31 and Dh44 (N=3).

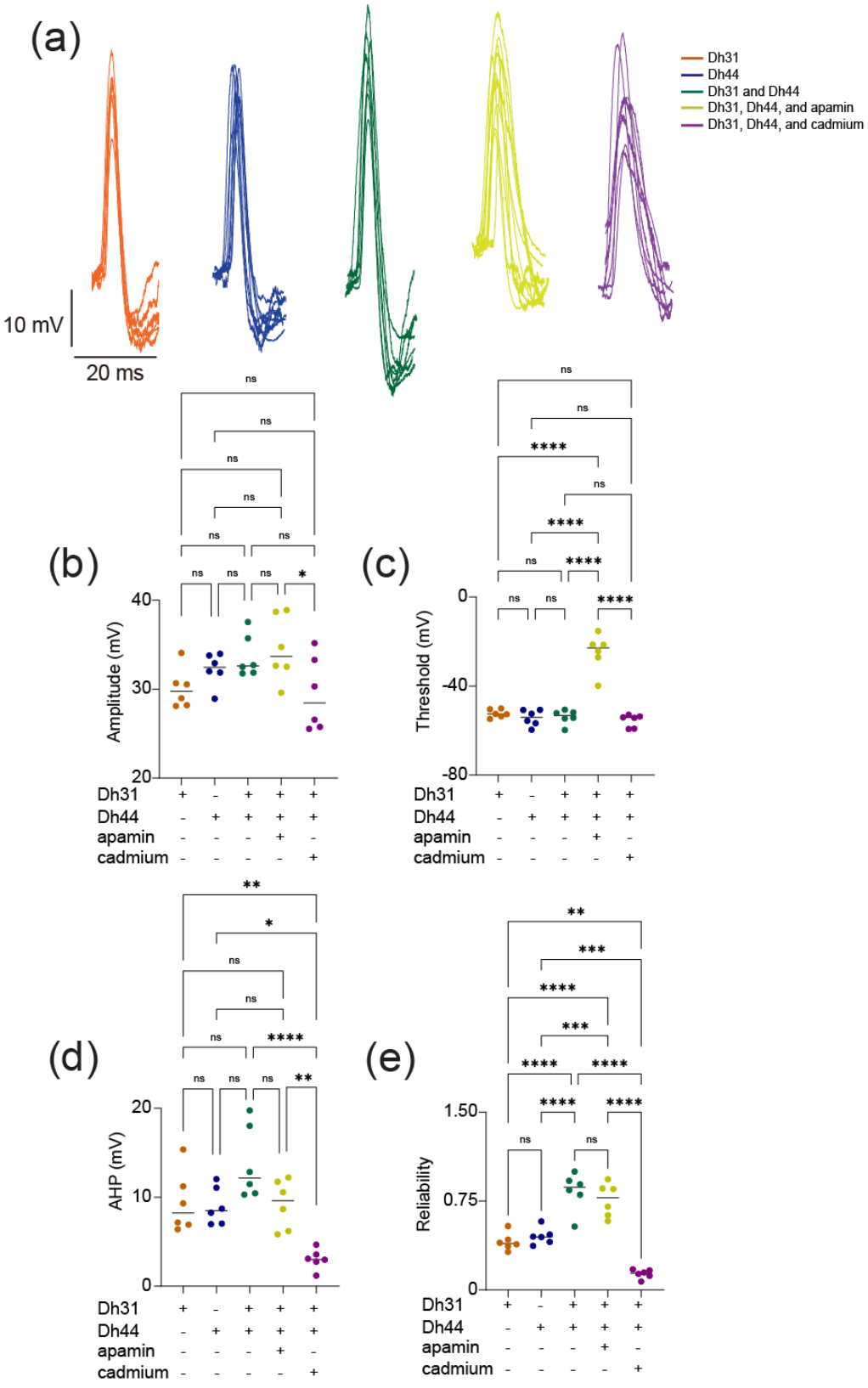

FIGURE 3

FIGURE 3 Spontaneous action potential waveform change during the applications of Dh31/Dh44. **(a)** Voltage traces showing action potential waveform changes by Dh31, Dh44, Dh31/Dh44, Dh31/Dh44/apamin, and Dh31/Dh44/cadmium. **(b)** Quantification of action potential amplitude for varying conditions with (+) and without (-) Dh31, Dh44, apamin, and cadmium (N=6 each) **(c)** Quantification of action potential threshold for varying conditions with (+) and without (-) Dh31, Dh44, apamin, and cadmium (N=6 each). **(d)** Afterhyperpolarization (AHP) amplitude for varying conditions with (+) and without (-) Dh31, Dh44, apamin, and cadmium (N=6 each). **(e)** Quantification of reliability for varying conditions with (+) and without (-) Dh31, Dh44, apamin, and cadmium (N=6 each). To compare more than two multiple-group comparisons, one-way ANOVA with multiple comparisons was used. A p-value < 0.05 was considered statistically significant, with asterisks indicating p-values as follows: $^{*}p < 0.05$, $^{**}p < 0.01$, $^{***}p < 0.001$, and $^{****}p < 0.0001$.

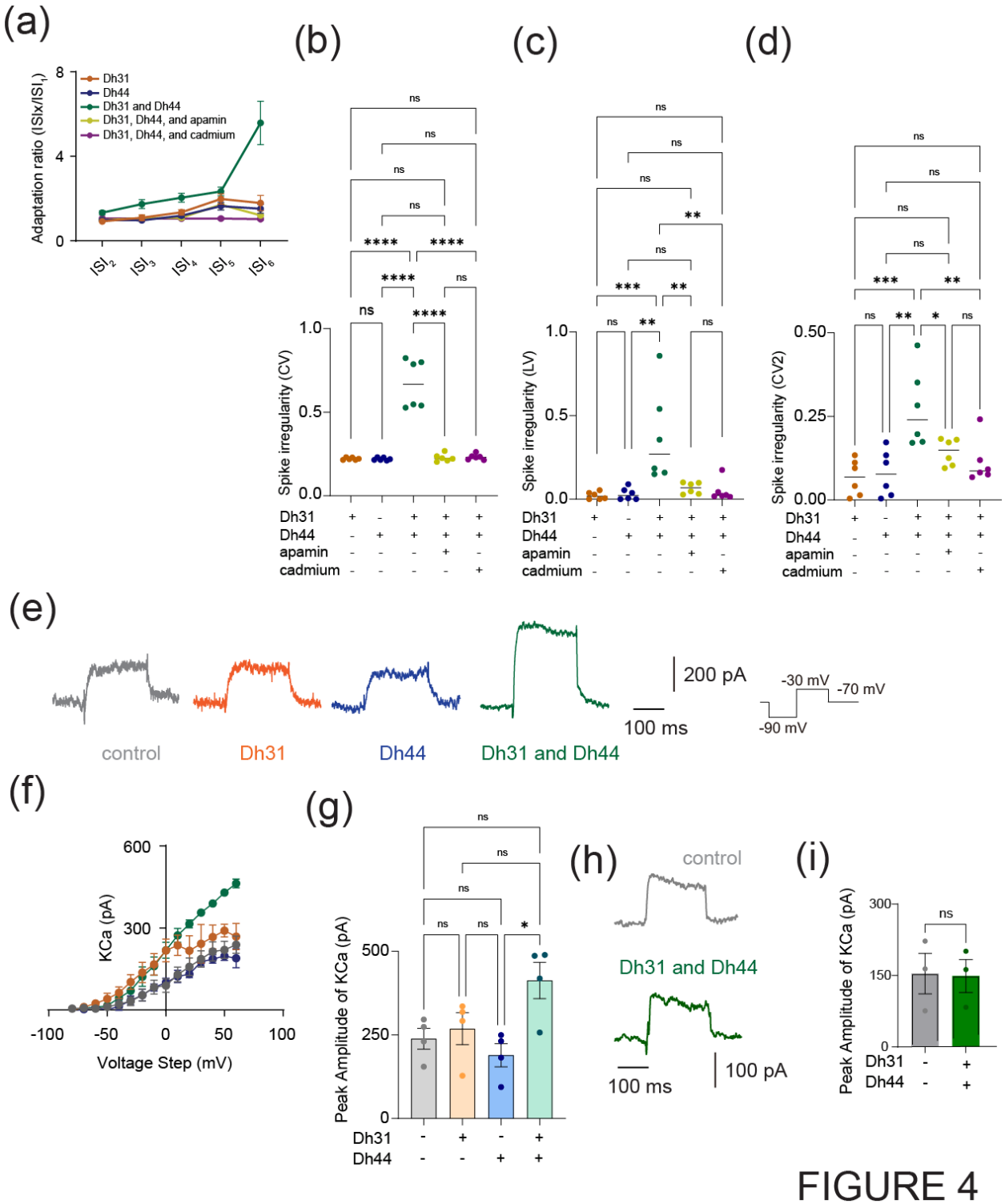

FIGURE 4

FIGURE 4 Dh31/Dh44-induced changes in spike pattern and KCa channel conductance. **(a)** Quantification of spike frequency adaptation with ISIx/ISI$_1$ ratio for Dh31, Dh44, Dh31 and Dh44, Dh31/Dh44/apamin, and Dh31/Dh44/cadmium (N=5). **(b-d)** Quantification of spike irregularity of CV, LV, and CV2 for varying conditions with (+) and without (-) Dh31, Dh44, apamin, and

cadmium (N=6 each). **(e)** Current traces of control, Dh31, Dh44, and Dh31/Dh44. **(f)** I-V relationship of KCa conductance and peak amplitude of K_{Ca} for control, Dh31, Dh44, and Dh31/Dh44 (n=4 each). **(g)** Quantification of Peak Amplitude of KCa for varying conditions with (+) and without (-) Dh31, Dh44, apamin, and cadmium (N=4 each). **(h)** Current traces of control and both Dh31 and Dh44 together. **(i)** Quantification of Peak Amplitude KCa for control and both Dh31 and Dh44 together. One-way ANOVA with multiple comparisons was used. A p-value < 0.05 was considered statistically significant, with asterisks indicating p-values as follows: $^{*}p < 0.05$, $^{**}p < 0.01$, $^{***}p < 0.001$, and $^{****}p < 0.0001$.

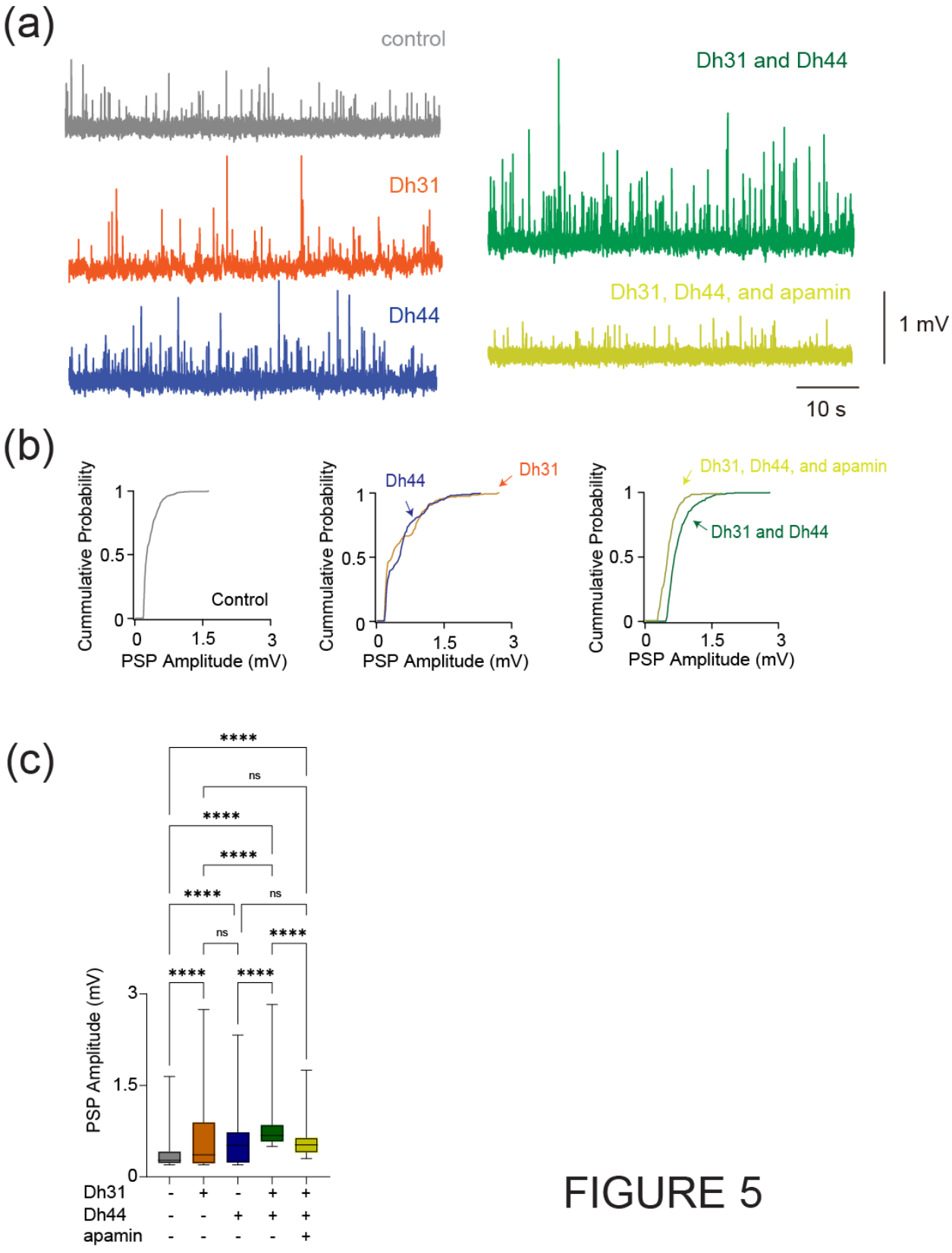

FIGURE 5

FIGURE 5 Changes in synaptic potential induced by Dh31/Dh44. **(a)** Voltage traces showing

synaptic potential sequence changes for control, Dh31, Dh44, Dh31/Dh44, and Dh31/Dh44/apamin. **(b)** Cumulative probability of PSP for control, Dh31, Dh44, Dh31/Dh44, and Dh31/Dh44/apamin.**(c)** Quantification of postsynaptic potential (PSP) amplitude for varying conditions with (+) and without (-) Dh31, Dh44, and apamin. One-way ANOVA with multiple comparisons was used for the statistics with $^{***}p < 0.001$, and $^{****}p < 0.0001$.

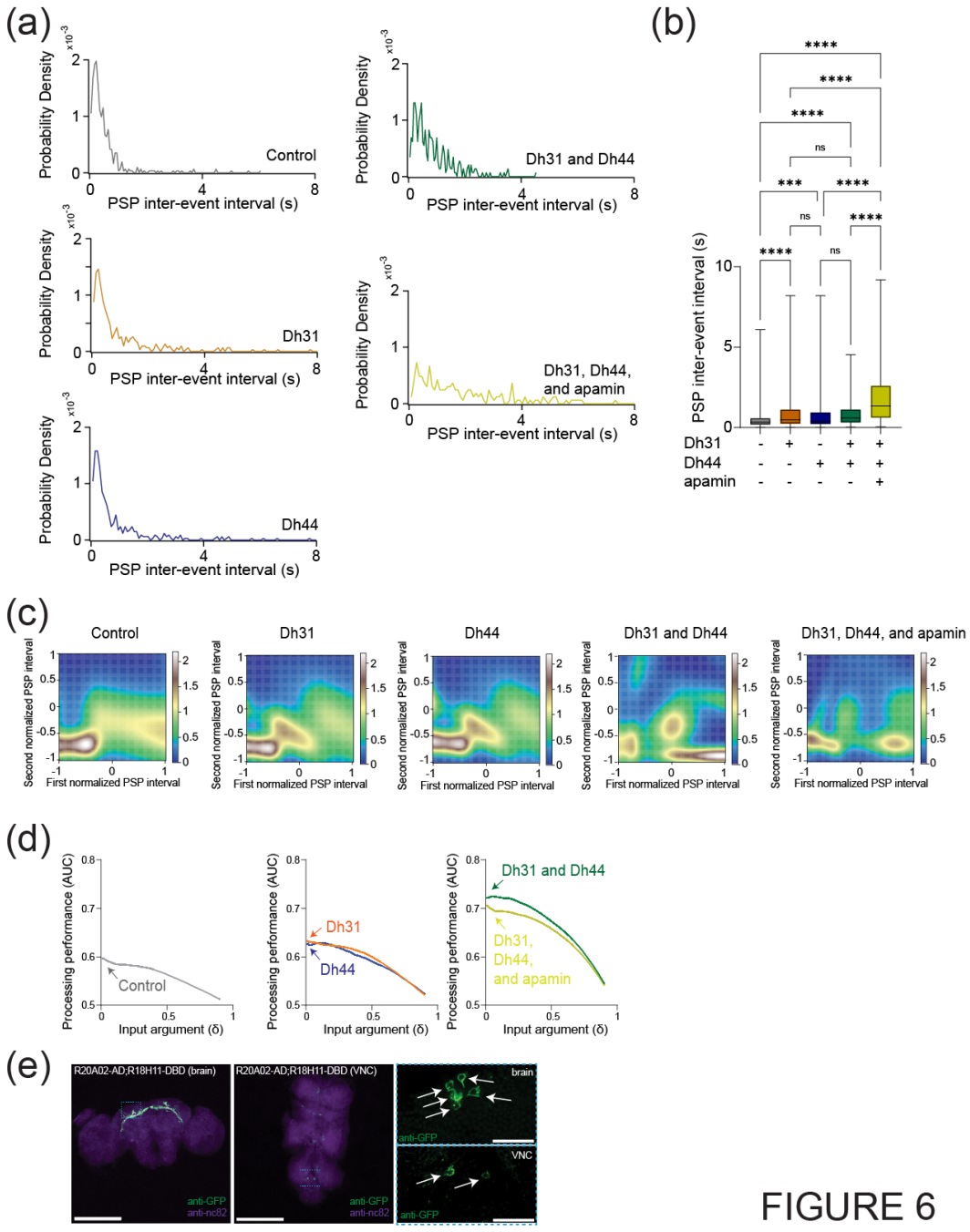

FIGURE 6

FIGURE 6 Synaptic potentials show complex patterns under Dh31/Dh44 influence and possible involvement of Dh31-positive DN1 clock neurons. **(a)** Probability density of PSP inter event intervals for control (N=3), Dh31 (N=3), Dh44 (N=30), Dh31/Dh44 (N=3), and

Dh31/Dh44/apamin (N=4). **(b)** Time between each event, PSP inter-event interval, was quantified from conditions with (+) and without (-) Dh31, Dh44, and apamin. **(c)** The interval times of two adjacent PSPs were projected into two-dimensional space, and Gaussian Mixture Model (GMM) was used to computationally capture the geometry of their probability distribution. (**d**) The area under the curve (AUC) in receiver operating characteristic (ROC) analysis based on interval timing of PSPs in PI neurons. (**e**) Whole-mount brain (left) and thoracic ganglion (right) immunostaining of a *R20A02-AD;R18H11-DBD>UAS-thGFP* fly with anti-GFP (green) and anti-nc82 (magenta). Scale bar indicates 300 μm and 30 μm in inset. The statistics used were unpaired t-test with *p < 0.05 and **p < 0.01 and ns indicated non-significant.

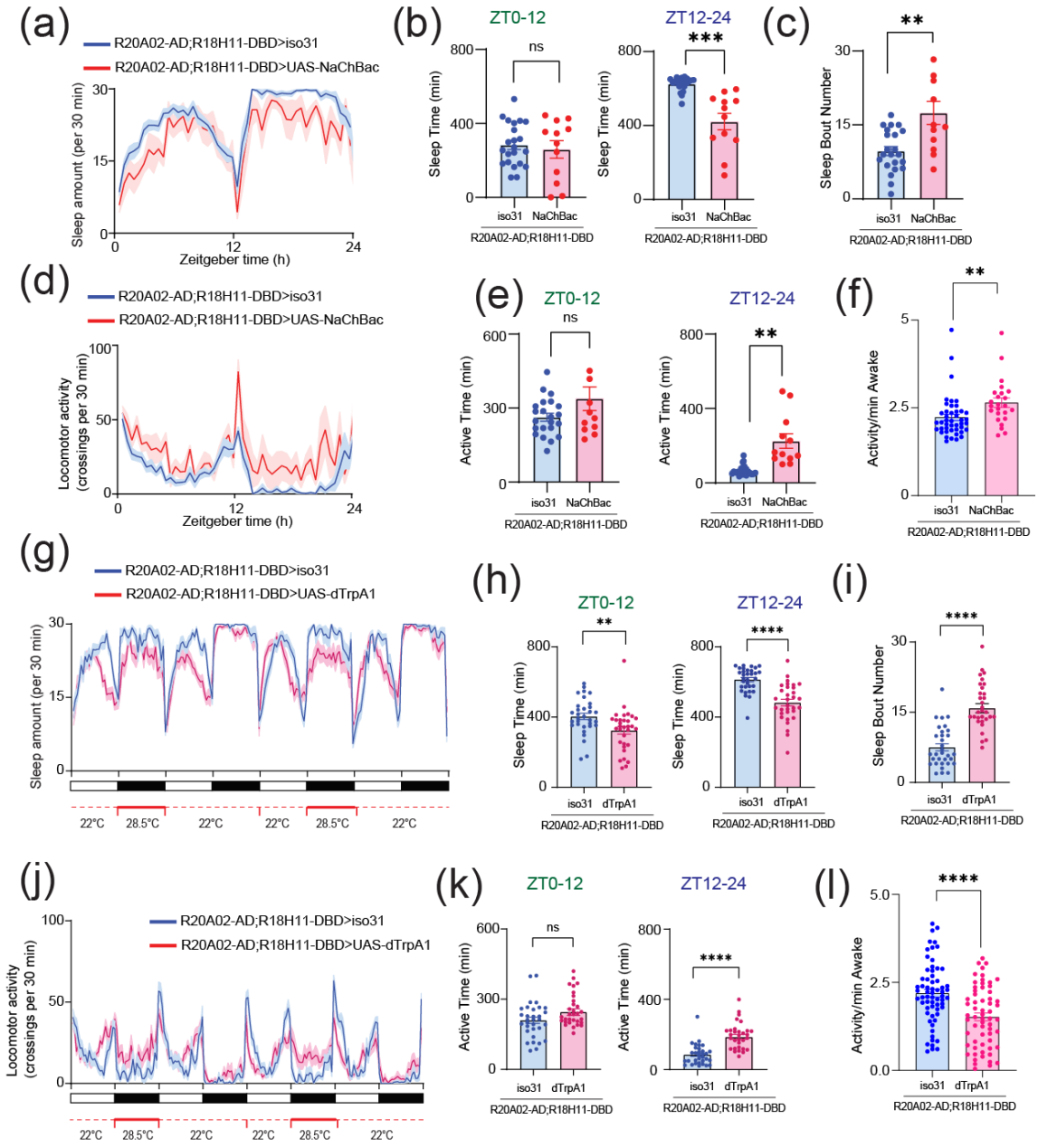

FIGURE 7

FIGURE 7 (a) Sleep profiles **(b)** Sleep time at ZT0-12 and ZT12-24 **(c)** Sleep bout number of *R20A02-AD;R18H11-DBD>iso31* (blue, N=23) and *R20A02-AD;R18H11-DBD>UAS-NaChBac* (red, N=12) flies. Sleep time plotted in 30 min bins. (**d**) Activity profiles (**e**) Active time at ZT0-12 and ZT12-24 (**f**) Daily waking activity of *R20A02-AD;R18H11-DBD>iso31* (blue) and *R20A02-AD;R18H11-DBD>UAS-NaChBac* (red) flies. (**g**) Sleep profiles (**h**) Sleep time at ZT0-12 and ZT12-24 (**i**) Sleep bout number of *R20A02-AD;R18H11-DBD>iso31* (blue) and *R20A02-AD;R18H11-DBD>UAS- dTRPA1* (red) flies. (**j**) Activity profiles (**k**) Active time at ZT0-12 and ZT12-24 (**l**) Daily waking activity of *R20A02-AD;R18H11-DBD>iso31* (blue) and *R20A02-AD;R18H11-DBD>UAS- dTRPA1* (red) flies. The statistics used were unpaired t-test with *p < 0.05 and **p < 0.01 and ns indicated non-significant.

REFERENCES

Axmacher, N. & Miles, R. (2004) Intrinsic cellular currents and the temporal precision of EPSP-action potential coupling in CA1 pyramidal cells. *J Physiol*, **555**, 713-725.

Barber, A.F., Erion, R., Holmes, T.C. & Sehgal, A. (2016) Circadian and feeding cues integrate to drive rhythms of physiology in Drosophila insulin-producing cells. *Genes Dev*, **30**, 2596-2606.

Barber, A.F., Fong, S.Y., Kolesnik, A., Fetchko, M. & Sehgal, A. (2021) Drosophila clock cells use multiple mechanisms to transmit time-of-day signals in the brain. *Proc Natl Acad Sci U S A*, **118**.

Benda, J., Longtin, A. & Maler, L. (2005) Spike-frequency adaptation separates transient communication signals from background oscillations. *J Neurosci*, **25**, 2312-2321.

Benguettat, O., Jneid, R., Soltys, J., Loudhaief, R., Brun-Barale, A., Osman, D. & Gallet, A. (2018) The DH31/CGRP enteroendocrine peptide triggers intestinal contractions favoring the elimination of opportunistic bacteria. *PLoS Pathog*, **14**, e1007279.

Brette, R. (2015) Philosophy of the Spike: Rate-Based vs. Spike-Based Theories of the Brain. *Front Syst Neurosci*, **9**, 151.

Brown, S.A. & Schibler, U. (1999) The ins and outs of circadian timekeeping. *Curr Opin Genet Dev*, **9**, 588-594.

Buhr, E.D. & Takahashi, J.S. (2013) Molecular components of the Mammalian circadian clock. *Handb Exp Pharmacol*, 3-27.

Cavanaugh, D.J., Geratowski, J.D., Wooltorton, J.R., Spaethling, J.M., Hector, C.E., Zheng, X., Johnson, E.C., Eberwine, J.H. & Sehgal, A. (2014) Identification of a circadian output circuit for rest:activity rhythms in Drosophila. *Cell*, **157**, 689-701.

Cavey, M., Collins, B., Bertet, C. & Blau, J. (2016) Circadian rhythms in neuronal activity propagate through output circuits. *Nat Neurosci*, **19**, 587-595.

Cedernaes, J., Waldeck, N. & Bass, J. (2019) Neurogenetic basis for circadian regulation of metabolism by the hypothalamus. *Genes Dev*, **33**, 1136-1158.

Cederroth, C.R., Albrecht, U., Bass, J., Brown, S.A., Dyhrfjeld-Johnsen, J., Gachon, F., Green, C.B., Hastings, M.H., Helfrich-Forster, C., Hogenesch, J.B., Levi, F., Loudon, A., Lundkvist, G.B., Meijer, J.H., Rosbash, M., Takahashi, J.S., Young, M. & Canlon, B. (2019) Medicine in the Fourth Dimension. *Cell Metab*, **30**, 238-250.

Chen, J., Reiher, W., Hermann-Luibl, C., Sellami, A., Cognigni, P., Kondo, S., Helfrich-Forster, C., Veenstra, J.A. & Wegener, C. (2016) Allatostatin A Signalling in Drosophila Regulates Feeding and Sleep and Is Modulated by PDF. *PLoS Genet*, **12**, e1006346.

Chini, M., Pfeffer, T. & Hanganu-Opatz, I. (2022) An increase of inhibition drives the developmental decorrelation of neural activity. *Elife*, **11**.

Cloues, R.K. & Sather, W.A. (2003) Afterhyperpolarization regulates firing rate in neurons of the suprachiasmatic nucleus. *J Neurosci*, **23**, 1593-1604.

Colwell, C.S. (2011) Linking neural activity and molecular oscillations in the SCN. *Nat Rev Neurosci*, **12**, 553-569.

Corbacioglu, S.K. & Aksel, G. (2023) Receiver operating characteristic curve analysis in diagnostic accuracy studies: A guide to interpreting the area under the curve value. *Turk J Emerg Med*, **23**, 195-198.

Cui, E.D., Estright, A.W., Pressler, R.T. & Strowbridge, B.W. (2022) Spike Afterhyperpolarizations Govern Persistent Firing Dynamics in Rat Neocortical and Hippocampal Pyramidal Cells. *J Neurosci*, **42**, 7690-7706.

Dallmann, R., Viola, A.U., Tarokh, L., Cajochen, C. & Brown, S.A. (2012) The human circadian metabolome. *Proc Natl Acad Sci U S A*, **109**, 2625-2629.

Dionne, H., Hibbard, K.L., Cavallaro, A., Kao, J.C. & Rubin, G.M. (2018) Genetic Reagents for Making Split-GAL4 Lines in Drosophila. *Genetics*, **209**, 31-35.

Dubowy, C. & Sehgal, A. (2017) Circadian Rhythms and Sleep in Drosophila melanogaster. *Genetics*, **205**, 1373-1397.

761 Dumenieu, M., Fourcaud-Trocme, N., Garcia, S. & Kuczewski, N. (2015) Afterhyperpolarization (AHP)
762 regulates the frequency and timing of action potentials in the mitral cells of the olfactory bulb:
763 role of olfactory experience. *Physiol Rep*, **3**.

764

765 Dunlap, J.C. (1999) Molecular bases for circadian clocks. *Cell*, **96**, 271-290.

766

767 Dus, M., Lai, J.S., Gunapala, K.M., Min, S., Tayler, T.D., Hergarden, A.C., Geraud, E., Joseph, C.M. & Suh,
768 G.S. (2015) Nutrient Sensor in the Brain Directs the Action of the Brain-Gut Axis in Drosophila.
769 *Neuron*, **87**, 139-151.

770

771 Engbers, J.D., Anderson, D., Asmara, H., Rehak, R., Mehaffey, W.H., Hameed, S., McKay, B.E., Kruskic, M.,
772 Zamponi, G.W. & Turner, R.W. (2012) Intermediate conductance calcium-activated potassium
773 channels modulate summation of parallel fiber input in cerebellar Purkinje cells. *Proc Natl Acad*
774 *Sci U S A*, **109**, 2601-2606.

775

776 Franken, P. & Dijk, D.J. (2009) Circadian clock genes and sleep homeostasis. *Eur J Neurosci*, **29**, 1820-1829.

777

778 Gachon, F., Nagoshi, E., Brown, S.A., Ripperger, J. & Schibler, U. (2004) The mammalian circadian timing
779 system: from gene expression to physiology. *Chromosoma*, **113**, 103-112.

780

781 Gmeiner, F., Kolodziejczyk, A., Yoshii, T., Rieger, D., Nassel, D.R. & Helfrich-Forster, C. (2013) GABA(B)
782 receptors play an essential role in maintaining sleep during the second half of the night in
783 Drosophila melanogaster. *J Exp Biol*, **216**, 3837-3843.

784

785 Goda, T., Tang, X., Umezaki, Y., Chu, M.L., Kunst, M., Nitabach, M.N.N. & Hamada, F.N. (2016) Drosophila
786 DH31 Neuropeptide and PDF Receptor Regulate Night-Onset Temperature Preference. *J Neurosci*,
787 **36**, 11739-11754.

788

789 Goda, T., Umezaki, Y., Alwattari, F., Seo, H.W. & Hamada, F.N. (2019) Neuropeptides PDF and DH31
790 hierarchically regulate free-running rhythmicity in Drosophila circadian locomotor activity. *Sci Rep*,
791 **9**, 838.

792

793 Goltsev, A.V., Wright, E.A.P., Mendes, J.F.F. & Yoon, S. (2022) Generation and Disruption of Circadian
794 Rhythms in the Suprachiasmatic Nucleus: A Core-Shell Model. *J Biol Rhythms*, **37**, 545-561.

795

796 Gouwens, N.W. & Wilson, R.I. (2009) Signal propagation in Drosophila central neurons. *J Neurosci*, **29**,
797 6239-6249.

798

799 Green, C.B., Takahashi, J.S. & Bass, J. (2008) The meter of metabolism. *Cell*, **134**, 728-742.

800

801 Guo, F., Holla, M., Diaz, M.M. & Rosbash, M. (2018) A Circadian Output Circuit Controls Sleep-Wake

802 Arousal in Drosophila. *Neuron*, **100**, 624-635 e624.

803

804 Guo, F., Yu, J., Jung, H.J., Abruzzi, K.C., Luo, W., Griffith, L.C. & Rosbash, M. (2016) Circadian neuron
805 feedback controls the Drosophila sleep--activity profile. *Nature*, **536**, 292-297.

806

807 Hajian-Tilaki, K. (2013) Receiver Operating Characteristic (ROC) Curve Analysis for Medical Diagnostic Test
808 Evaluation. *Caspian J Intern Med*, **4**, 627-635.

809

810 Hamada, F.N., Rosenzweig, M., Kang, K., Pulver, S.R., Ghezzi, A., Jegla, T.J. & Garrity, P.A. (2008) An internal
811 thermal sensor controlling temperature preference in Drosophila. *Nature*, **454**, 217-220.

812

813 Hamasaka, Y., Rieger, D., Parmentier, M.L., Grau, Y., Helfrich-Forster, C. & Nassel, D.R. (2007) Glutamate
814 and its metabotropic receptor in Drosophila clock neuron circuits. *J Comp Neurol*, **505**, 32-45.

815

816 Hardin, P.E. & Panda, S. (2013) Circadian timekeeping and output mechanisms in animals. *Curr Opin*
817 *Neurobiol*, **23**, 724-731.

818

819 Hastings, M.H., Maywood, E.S. & Brancaccio, M. (2018) Generation of circadian rhythms in the
820 suprachiasmatic nucleus. *Nat Rev Neurosci*, **19**, 453-469.

821

822 Hausdorff, J.M. & Peng, C. (1996) Multiscaled randomness: A possible source of 1/f noise in biology. *Phys*
823 *Rev E Stat Phys Plasmas Fluids Relat Interdiscip Topics*, **54**, 2154-2157.

824

825 Helfrich-Forster, C. (2003) The neuroarchitecture of the circadian clock in the brain of Drosophila
826 melanogaster. *Microsc Res Tech*, **62**, 94-102.

827

828 Hermann-Luibl, C., Yoshii, T., Senthilan, P.R., Dircksen, H. & Helfrich-Forster, C. (2014) The ion transport
829 peptide is a new functional clock neuropeptide in the fruit fly Drosophila melanogaster. *J Neurosci*,
830 **34**, 9522-9536.

831

832 Herzog, E.D. & Schwartz, W.J. (2002) A neural clockwork for encoding circadian time. *J Appl Physiol (1985)*,
833 **92**, 401-408.

834

835 Hill, V.M., O'Connor, R.M. & Shirasu-Hiza, M. (2020) Tired and stressed: Examining the need for sleep. *Eur*
836 *J Neurosci*, **51**, 494-508.

837

838 Holt, G.R., Softky, W.R., Koch, C. & Douglas, R.J. (1996) Comparison of discharge variability in vitro and in
839 vivo in cat visual cortex neurons. *Journal of neurophysiology*, **75**, 1806-1814.

840

841 Huang, W., Ramsey, K.M., Marcheva, B. & Bass, J. (2011) Circadian rhythms, sleep, and metabolism. *J Clin*

Invest, **121**, 2133-2141.

Jameson, A.T., Spera, L.K., Nguyen, D.L., Paul, E.M. & Tabuchi, M. (2024) Membrane-coated glass electrodes for stable, low-noise electrophysiology recordings in Drosophila central neurons. *J Neurosci Methods*, 110079.

Jedema, H.P. & Grace, A.A. (2004) Corticotropin-releasing hormone directly activates noradrenergic neurons of the locus ceruleus recorded in vitro. *J Neurosci*, **24**, 9703-9713.

Jepson, J., Sheldon, A., Shahidullah, M., Fei, H., Koh, K. & Levitan, I.B. (2013) Cell-specific fine-tuning of neuronal excitability by differential expression of modulator protein isoforms. *J Neurosci*, **33**, 16767-16777.

Joiner, W.J., Crocker, A., White, B.H. & Sehgal, A. (2006) Sleep in Drosophila is regulated by adult mushroom bodies. *Nature*, **441**, 757-760.

King, A.N., Barber, A.F., Smith, A.E., Dreyer, A.P., Sitaraman, D., Nitabach, M.N., Cavanaugh, D.J. & Sehgal, A. (2017) A Peptidergic Circuit Links the Circadian Clock to Locomotor Activity. *Curr Biol*, **27**, 1915-1927 e1915.

King, A.N. & Sehgal, A. (2020) Molecular and circuit mechanisms mediating circadian clock output in the Drosophila brain. *Eur J Neurosci*, **51**, 268-281.

Klose, M.K., Bruchez, M.P., Deitcher, D.L. & Levitan, E.S. (2021) Temporally and spatially partitioned neuropeptide release from individual clock neurons. *Proc Natl Acad Sci U S A*, **118**.

Kostal, L. & Lansky, P. (2007) Variability and randomness in stationary neuronal activity. *Biosystems*, **89**, 44-49.

Kostal, L., Lansky, P. & Rospars, J.P. (2007) Neuronal coding and spiking randomness. *Eur J Neurosci*, **26**, 2693-2701.

Kostal, L. & Marsalek, P. (2010) Neuronal jitter: can we measure the spike timing dispersion differently? *Chin J Physiol*, **53**, 454-464.

Kunst, M., Hughes, M.E., Raccuglia, D., Felix, M., Li, M., Barnett, G., Duah, J. & Nitabach, M.N. (2014) Calcitonin gene-related peptide neurons mediate sleep-specific circadian output in Drosophila. *Curr Biol*, **24**, 2652-2664.

Kurogi, Y., Imura, E., Mizuno, Y., Hoshino, R., Nouzova, M., Matsuyama, S., Mizoguchi, A., Kondo, S., Tanimoto, H., Noriega, F.G. & Niwa, R. (2023) Female reproductive dormancy in Drosophila is

883 regulated by DH31-producing neurons projecting into the corpus allatum. *Development*, **150**.

884

885 Lamaze, A., Kratschmer, P., Chen, K.F., Lowe, S. & Jepson, J.E.C. (2018) A Wake-Promoting Circadian
886 Output Circuit in Drosophila. *Curr Biol*, **28**, 3098-3105 e3093.

887

888 Lee, G., Jang, H. & Oh, Y. (2023a) The role of diuretic hormones (DHs) and their receptors in Drosophila.
889 *BMB Rep*, **56**, 209-215.

890

891 Lee, H., Kostal, L., Kanzaki, R. & Kobayashi, R. (2023b) Spike frequency adaptation facilitates the encoding
892 of input gradient in insect olfactory projection neurons. *Biosystems*, **223**, 104802.

893

894 Lelito, K.R. & Shafer, O.T. (2012) Reciprocal cholinergic and GABAergic modulation of the small
895 ventrolateral pacemaker neurons of Drosophila's circadian clock neuron network. *J Neurophysiol*,
896 **107**, 2096-2108.

897

898 Levakova, M., Tamborrino, M., Kostal, L. & Lansky, P. (2016) Presynaptic Spontaneous Activity Enhances
899 the Accuracy of Latency Coding. *Neural Comput*, **28**, 2162-2180.

900

901 Liang, X., Ho, M.C.W., Zhang, Y., Li, Y., Wu, M.N., Holy, T.E. & Taghert, P.H. (2019) Morning and Evening
902 Circadian Pacemakers Independently Drive Premotor Centers via a Specific Dopamine Relay.
903 *Neuron*, **102**, 843-857 e844.

904

905 Liu, S., Lamaze, A., Liu, Q., Tabuchi, M., Yang, Y., Fowler, M., Bharadwaj, R., Zhang, J., Bedont, J., Blackshaw,
906 S., Lloyd, T.E., Montell, C., Sehgal, A., Koh, K. & Wu, M.N. (2014) WIDE AWAKE mediates the
907 circadian timing of sleep onset. *Neuron*, **82**, 151-166.

908

909 Lowe, S.A., Wilson, A.D., Aughey, G.N., Banerjee, A., Goble, T., Simon-Batsford, N., Sanderson, A.,
910 Kratschmer, P., Balogun, M., Gao, H., Aw, S.S. & Jepson, J.E.C. (2024) Modulation of a critical
911 period for motor development in Drosophila by BK potassium channels. *Curr Biol*, **34**, 3488-3505
912 e3483.

913

914 Lyu, S., Terao, N., Nakashima, H., Itoh, M. & Tonoki, A. (2023) Neuropeptide diuretic hormone 31 mediates
915 memory and sleep via distinct neural pathways in Drosophila. *Neurosci Res*, **192**, 11-25.

916

917 Maejima, T., Ohno-Shosaku, T. & Kano, M. (2001) Endogenous cannabinoid as a retrograde messenger
918 from depolarized postsynaptic neurons to presynaptic terminals. *Neurosci Res*, **40**, 205-210.

919

920 Maury, E., Hong, H.K. & Bass, J. (2014) Circadian disruption in the pathogenesis of metabolic syndrome.
921 *Diabetes Metab*, **40**, 338-346.

922

923 McCarthy, E.V., Wu, Y., Decarvalho, T., Brandt, C., Cao, G. & Nitabach, M.N. (2011) Synchronized bilateral

924 synaptic inputs to Drosophila melanogaster neuropeptidergic rest/arousal neurons. *J Neurosci*, **31**,
925 8181-8193.

926
927 Mertens, I., Vandingenen, A., Johnson, E.C., Shafer, O.T., Li, W., Trigg, J.S., De Loof, A., Schoofs, L. &
928 Taghert, P.H. (2005) PDF receptor signaling in Drosophila contributes to both circadian and
929 geotactic behaviors. *Neuron*, **48**, 213-219.

930
931 Mohawk, J.A. & Takahashi, J.S. (2011) Cell autonomy and synchrony of suprachiasmatic nucleus circadian
932 oscillators. *Trends Neurosci*, **34**, 349-358.

933
934 Mountoufaris, G., Nair, A., Yang, B., Kim, D.W., Vinograd, A., Kim, S., Linderman, S.W. & Anderson, D.J.
935 (2024) A line attractor encoding a persistent internal state requires neuropeptide signaling. *Cell*.

936
937 Naundorf, B., Wolf, F. & Volgushev, M. (2006) Unique features of action potential initiation in cortical
938 neurons. *Nature*, **440**, 1060-1063.

939
940 Nguyen, D.L., Hutson, A.N., Zhang, Y., Daniels, S.D., Peard, A.R. & Tabuchi, M. (2022) Age-Related
941 Unstructured Spike Patterns and Molecular Localization in Drosophila Circadian Neurons. *Front*
942 *Physiol*, **13**, 845236.

943
944 Niday, Z. & Bean, B.P. (2021) BK Channel Regulation of Afterpotentials and Burst Firing in Cerebellar
945 Purkinje Neurons. *J Neurosci*, **41**, 2854-2869.

946
947 Nitabach, M.N. & Taghert, P.H. (2008) Organization of the Drosophila circadian control circuit. *Curr Biol*,
948 **18**, R84-93.

949
950 Oh, Y. & Suh, G.S.B. (2023) Starvation-induced sleep suppression requires the Drosophila brain nutrient
951 sensor. *J Neurogenet*, **37**, 70-77.

952
953 Ono, D., Mukai, Y., Hung, C.J., Chowdhury, S., Sugiyama, T. & Yamanaka, A. (2020) The mammalian
954 circadian pacemaker regulates wakefulness via CRF neurons in the paraventricular nucleus of the
955 hypothalamus. *Sci Adv*, **6**.

956
957 Panda, S. (2016) Circadian physiology of metabolism. *Science*, **354**, 1008-1015.

958
959 Parisky, K.M., Agosto, J., Pulver, S.R., Shang, Y., Kuklin, E., Hodge, J.J., Kang, K., Liu, X., Garrity, P.A., Rosbash,
960 M. & Griffith, L.C. (2008) PDF cells are a GABA-responsive wake-promoting component of the
961 Drosophila sleep circuit. *Neuron*, **60**, 672-682.

962
963 Poe, A.R., Zhu, L., Szuperak, M., McClanahan, P.D., Anafi, R.C., Scholl, B., Thum, A.S., Cavanaugh, D.J. &
964 Kayser, M.S. (2023) Developmental emergence of sleep rhythms enables long-term memory in

Drosophila. *Sci Adv*, **9**, eadh2301.

Ruiz, D., Bajwa, S.T., Vanani, N., Bajwa, T.A. & Cavanaugh, D.J. (2021) Slowpoke functions in circadian output cells to regulate rest:activity rhythms. *PLoS One*, **16**, e0249215.

Sahu, G. & Turner, R.W. (2021) The Molecular Basis for the Calcium-Dependent Slow Afterhyperpolarization in CA1 Hippocampal Pyramidal Neurons. *Front Physiol*, **12**, 759707.

Salaj, D., Subramoney, A., Kraisnikovic, C., Bellec, G., Legenstein, R. & Maass, W. (2021) Spike frequency adaptation supports network computations on temporally dispersed information. *Elife*, **10**.

Schlichting, M., Menegazzi, P., Lelito, K.R., Yao, Z., Buhl, E., Dalla Benetta, E., Bahle, A., Denike, J., Hodge, J.J., Helfrich-Forster, C. & Shafer, O.T. (2016) A Neural Network Underlying Circadian Entrainment and Photoperiodic Adjustment of Sleep and Activity in Drosophila. *J Neurosci*, **36**, 9084-9096.

Schwarz, J.E., King, A.N., Hsu, C.T., Barber, A.F. & Sehgal, A. (2021) Hugin(+) neurons provide a link between sleep homeostat and circadian clock neurons. *Proc Natl Acad Sci U S A*, **118**.

Scuri, R., Mozzachiodi, R. & Brunelli, M. (2005) Role for calcium signaling and arachidonic acid metabolites in the activity-dependent increase of AHP amplitude in leech T sensory neurons. *J Neurophysiol*, **94**, 1066-1073.

Shafer, O.T. & Keene, A.C. (2021) The Regulation of Drosophila Sleep. *Curr Biol*, **31**, R38-R49.

Shafer, O.T., Kim, D.J., Dunbar-Yaffe, R., Nikolaev, V.O., Lohse, M.J. & Taghert, P.H. (2008) Widespread receptivity to neuropeptide PDF throughout the neuronal circadian clock network of Drosophila revealed by real-time cyclic AMP imaging. *Neuron*, **58**, 223-237.

Shahidullah, M., Reddy, S., Fei, H. & Levitan, I.B. (2009) In vivo role of a potassium channel-binding protein in regulating neuronal excitability and behavior. *J Neurosci*, **29**, 13328-13337.

Shang, Y., Donelson, N.C., Vecsey, C.G., Guo, F., Rosbash, M. & Griffith, L.C. (2013) Short neuropeptide F is a sleep-promoting inhibitory modulator. *Neuron*, **80**, 171-183.

Shinomoto, S., Kim, H., Shimokawa, T., Matsuno, N., Funahashi, S., Shima, K., Fujita, I., Tamura, H., Doi, T., Kawano, K., Inaba, N., Fukushima, K., Kurkin, S., Kurata, K., Taira, M., Tsutsui, K., Komatsu, H., Ogawa, T., Koida, K., Tanji, J. & Toyama, K. (2009) Relating neuronal firing patterns to functional differentiation of cerebral cortex. *PLoS Comput Biol*, **5**, e1000433.

Shinomoto, S., Shima, K. & Tanji, J. (2003) Differences in spiking patterns among cortical neurons. *Neural computation*, **15**, 2823-2842.

Stiefel, K.M., Englitz, B. & Sejnowski, T.J. (2013) Origin of intrinsic irregular firing in cortical interneurons. *Proc Natl Acad Sci U S A*, **110**, 7886-7891.

Sun, X., Whitefield, S., Rusak, B. & Semba, K. (2001) Electrophysiological analysis of suprachiasmatic nucleus projections to the ventrolateral preoptic area in the rat. *Eur J Neurosci*, **14**, 1257-1274.

Tabuchi, M. (2024) Dynamic neuronal instability generates synaptic plasticity and behavior: Insights from Drosophila sleep. *Neurosci Res*, **198**, 1-7.

Tabuchi, M., Coates, K.E., Bautista, O.B. & Zukowski, L.H. (2021) Light/Clock Influences Membrane Potential Dynamics to Regulate Sleep States. *Front Neurol*, **12**, 625369.

Tabuchi, M., Monaco, J.D., Duan, G., Bell, B., Liu, S., Liu, Q., Zhang, K. & Wu, M.N. (2018) Clock-Generated Temporal Codes Determine Synaptic Plasticity to Control Sleep. *Cell*, **175**, 1213-1227 e1218.

Tomar, R. & Kostal, L. (2021) Variability and Randomness of the Instantaneous Firing Rate. *Front Comput Neurosci*, **15**, 620410.

Trinh, A.T., Clarke, S.E., Harvey-Girard, E. & Maler, L. (2019) Cellular and Network Mechanisms May Generate Sparse Coding of Sequential Object Encounters in Hippocampal-Like Circuits. *eNeuro*, **6**.

Turrigiano, G.G., Leslie, K.R., Desai, N.S., Rutherford, L.C. & Nelson, S.B. (1998) Activity-dependent scaling of quantal amplitude in neocortical neurons. *Nature*, **391**, 892-896.

Waschke, L., Wostmann, M. & Obleser, J. (2017) States and traits of neural irregularity in the age-varying human brain. *Sci Rep*, **7**, 17381.

Wegener, C., Hamasaka, Y. & Nassel, D.R. (2004) Acetylcholine increases intracellular Ca2+ via nicotinic receptors in cultured PDF-containing clock neurons of Drosophila. *J Neurophysiol*, **91**, 912-923.

Welsh, D.K., Takahashi, J.S. & Kay, S.A. (2010) Suprachiasmatic nucleus: cell autonomy and network properties. *Annu Rev Physiol*, **72**, 551-577.

Wilson, R.I. & Nicoll, R.A. (2001) Endogenous cannabinoids mediate retrograde signalling at hippocampal synapses. *Nature*, **410**, 588-592.

Wu, G., Ma, T., Hancock, C.E., Gonzalez, S., Aryal, B., Vaz, S., Chan, G., Palarca-Wong, M., Allen, N., Chung, C.-I., Shu, X. & Liu, Q. Opposing GPCR signaling programs protein intake setpoint in Drosophila. *Cell*.

Yang, D.P., Zhou, H.J. & Zhou, C. (2017) Co-emergence of multi-scale cortical activities of irregular firing, oscillations and avalanches achieves cost-efficient information capacity. *PLoS Comput Biol*, **13**, e1005384.